Determining the capability requirements

for a space-based optical sensor

to determine the trajectory of an incoming antisatellite weapon

THESIS

Mesut Gülmüş, First Lieutenant, TUAF

AFIT/GSS/ENY/08-M03

DEPARTMENT OF THE AIR FORCE

AIR UNIVERSITY

AIR FORCE INSTITUTE OF TECHNOLOGY

Wright-Patterson Air Force Base, Ohio

The views expressed in this thesis are those of the author and do not reflect the official policy or position of the United States Air Force, Department of Defense, or the United States Government.

AFIT/GSS/ENY/08-M03

Determining the capability requirements for a space-based optical sensor to determine the trajectory of an incoming antisatellite weapon

THESIS

Presented to the Faculty

Department of Aeronautics and Astronautics

Graduate School of Engineering and Management

Air Force Institute of Technology

Air University

Air Education and Training Command

In Partial Fulfillment of the Requirements for the

Degree of Master of Science in Space Systems

Mesut Gülmüş, B.S.A.E.

First Lieutenant, TUAF

March 2008

AFIT/GSS/ENY/08-M03

Determining the capability requirements for a space-based optical sensor to determine the trajectory of an incoming antisatellite weapon

Mesut Gülmüş, B.S.A.E.
First Lieutenant, TUAF

Approved:

/signed/	12 March 2008
Lt Col Kerry D. Hicks, (Chairman)	Date
/signed/	12 March 2008
Dr. William E. Wiesel (Member)	Date
/signed/	12 March 2008
Dr. Richard G. Cobb (Member)	Date

Abstract

The goal of this research is to build up a logic to catch and track incoming ASAT weapons by using space-based onboard optical sensors. The satellite orbit and ASAT trajectory of the Chinese test were generated to relate the research to the real world application. These position and velocity values are used to generate simulated observation data for a hypothetical sensor on the targeted satellite. These observation values are assumed to be true, and some representative amounts of error was added to these data. Only two body dynamics are considered; drag effect and other perturbations are neglected. The modern orbit determination process, least squares method, and Monte Carlo techniques are used to calculate the estimated orbit of the ASAT. Standard deviations of the relative position of the ASAT with respect to the targeted satellite at the time of impact are calculated for different sensors with different accuracy and data collection intervals.

Acknowledgements

First and foremost, I would like to thank my wife for supporting me in all cases and all times as well as we were in the United States of America. While I was studying in AFIT at weekends her precious understanding allowed me to concentrate to my research. I would also like to express my appreciation to Lt Col Kerry D Hicks for his ideas and teachings. He not only taught some data but also showed the proper way of using that data. His advice about the research led me in this innovative study.

Similarly, I would like to express my appreciation to Dr. William E Wiesel for his excellent willingness to teach the modern orbit determination. His orbit determination class itself provided me enough background for the theory of the research. Finally, as a foreign military student at AFIT, I would like to thank to all my American instructors and colleagues for their hospitality and kindness.

Mesut Gülmüş

Table of Contents

Page

List of Figures

List of Tables

List of Symbols

List of Abbreviations

Abbreviation		Page
HEO	Highly Elliptical Orbit	22
SBIRS	Space Based Infrared System	22
EOM	Equation of Motion	29

Determining the capability requirements for a space-based optical sensor to determine the trajectory of an incoming antisatellite weapon

I. Introduction

1.1 Problem Statement

On January 11, 2007, the People's Republic of China (PRC) conducted its first successful antisatellite (ASAT) weapons test and destroyed its own Fengyun-1C, a defunct weather satellite, in space. FY-1C was launched in 1999 and was orbiting the Earth in a polar, low Earth orbit (LEO) at an altitude of about 537 miles (865km), with a mass of about 750 kilograms. China used a modified DON FENG-21 road-mobile Intermediate Range Ballistic Missile (IRBM) with a 600 kg payload as an ASAT, pictured in Figure 1.1-(b). The ASAT missile was launched from China's Xichang Space Center, in Sichuan province, shown in Figure 1.1-(a). The Chinese government publicly confirmed that they had conducted the test on January 23, 2007. Figure 1.1-(c) represents the debris cloud created just after impact. The calculations and simulation of the test were done by Dr. T. S. Kelso and published on his official website. [6]

The test had two major and concerning results, affecting all countries. The first of which was the potentially damaging space debris as a result of the collision. After

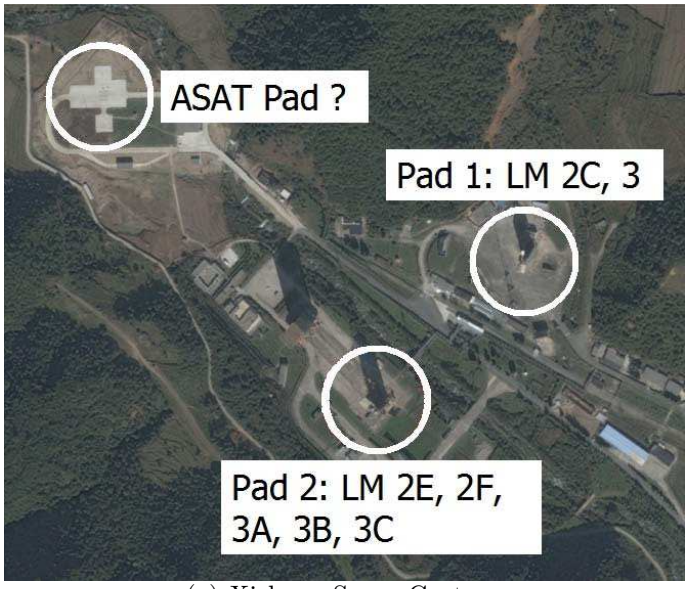

(a) Xichang Space Center.

(b) DON FENG-21

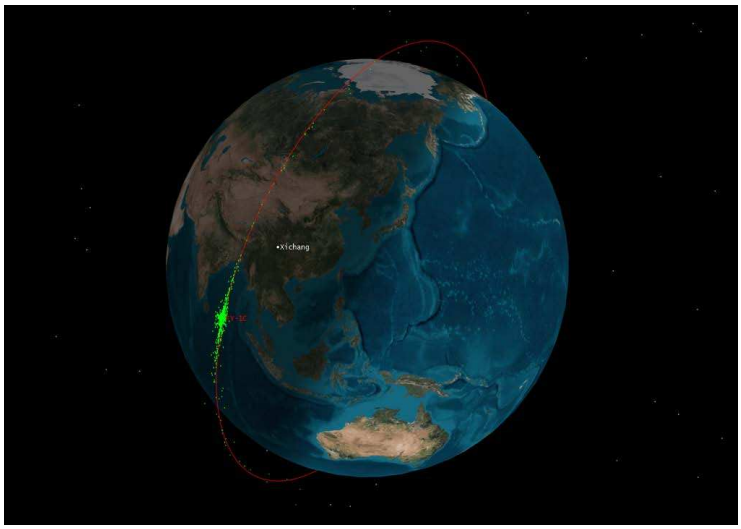

(c) Demonstration of Chinese ASAT test by AGI.

Figure 1.1: Chinese ASAT test. [6]

the test, the U.S. Space Surveillance Network tracked and cataloged 1337 pieces larger than 10 centimeters and an estimated minimum of 35000 additional smaller pieces were declared. The resulting debris spread from 200 kilometers to 4000 kilometers and began to endanger almost all LEO satellites and also the International Space Station (ISS), orbiting at an altitude of approximately 400 km. The Air Force Space Command declared that the space debris increased the collision risk for about 700 spacecraft. According to the optimistic calculations of Dr. Kelso from CelesTrack, after 100 years, only 15% of the total debris will be expected to have decayed. [6]

On the other hand, and more relevant to this thesis research, the test raised international concerns about China's capability and intention to attack satellites. This was the first destruction of a satellite with an ASAT after a long break since the Cold War. During the Cold War both the United States and the Soviet Union had conducted such ASAT tests. But since the 1980's neither of these countries, nor any other country, has intentionally destroyed satellites in space.

In such an arena where satellites can be threatened by kinetic energy weapons, precautionary actions become necessary again. Since it is an expensive, time consuming and time-sensitive process to put a payload into space and then to sustain it in order to get the advantage of the ultimate high ground, possessors of space systems should also take actions to protect the payloads. Finally, the problem appears to be seeing and avoiding a kinetic kill vehicle intended to damage or destroy the satellite.

1.2 Method of Solution

Optical sensors are commonly used on satellites especially for attitude determination and control subsystems of the payloads. Can we find a way or build up a logic to catch and track the incoming ASAT weapons by using these already onboard optical sensors? The goal of this research is to find the answer to this question. The satellite orbit and ASAT trajectory of the Chinese test were generated to relate the research to the real world application. These position and velocity values are used to generate simulated observation data for a hypothetical sensor on the targeted satellite. These observation values are assumed to be true, and representative amounts of error is added to these data. A modern orbit determination process, least squares method, and Monte Carlo techniques are used to calculate the estimated orbit of the ASAT. Standard deviations of the relative position of the ASAT with respect to the targeted satellite at the time of impact are calculated for different sensors with different accuracy and data collection intervals.

1.3 Organization

- Chapter 1: Introduces the problem and research goals.
- Chapter 2: Provides a comprehensive problem background and examines what has been done to address the problem area.
- Chapter 3: Explicitly details the problem solving approach. Includes an experimental method description, the tools and techniques developed, and approach verification/validation.

- Chapter 4: Discusses and provides the results. Interprets what the results mean and how they correlate to each other.
- Chapter 5: Covers the research conclusions and major result trends. Provides recommendations for future research.
- Appendices: $MATLAB$ code supporting the simulations/experiments.

II. Background and Literature Review

While inspecting the background of the research, a synopsis of the previous and current implementations on space weapons, space surveillance, sensors for ballistic missile defense and previous research will be beneficial.

2.1 ASAT History

An antisatellite weapon can be defined as any weapon system, whether land-based, sea-based, airborne, or space-based, which is specifically designed and intended to destroy, damage or interfere with the normal functioning of space objects. Beside the psychological effects on the enemy, space's initial military use was reconnaissance. During the oversensitive years of cold-war, Sputnik I represented the idea of Russian superiority in space technology when it was first launched in 1957. The launch of Sputnik also triggered the desire for the development of an ASAT weapon. The first official project of the Advanced Research Planning Agency (ARPA) was named Project Defender, covering defense from both satellites and ballistic missiles. The US Air Force's Air Research and Development Command (ARDC) signed a contract with ARPA for the "study of weapon systems to combat hostile satellites" in 1958. Later NASA was involved in the act of researching ASAT and ballistic missile defense (BMD) technology. In the 1960's, anti-satellite capabilities were developed as part of the Soviet space defense program. They began development of a limited missile defense of Moscow, which employs nuclear-tipped interceptors. [8]

The very first ASATs were ballistic missile launched weapons with either non-nuclear or nuclear warheads. These were either direct hit-to-kill devices, or satellites with proximity fuses which would explode using debris particles to destroy the target satellite. In the case of using an ASAT with a nuclear warhead, the thermal blast, x-rays, other radiation effects, or electro-magnetic effects would be the kill mechanism. An early Russian ASAT was a multi-staged rocket with a small ground-controlled satellite with direct hit-to-kill capability. A self-guided homing vehicle was tried using infrared homing, but the system failed several times in testing, was not successful in the 60's, and was dropped. [8]

The US High Altitude Nuclear Test Program was a study to determine the effects of a nuclear warhead explosion in space. The purpose of Project Argus was to study the behavior of free electrons in the earth's magnetic field. The US military was also exploring the effect of nuclear explosions on the Explorer IV satellite, which would be used to monitor the tests. Three nuclear weapons carried by rockets were detonated in 1958. Project Argus showed that a nuclear explosion in space generates high energy radiation including particles from the explosion, the high energy electrons generate radio noise, and radio transmissions are affected. Also, it was observed that the electrons striking the metal surfaces of satellites can damage electronics. During a following Fishbowl project, a 1.4 megaton warhead exploded at an altitude of 248 miles and caused considerable interruption with Pacific communications, and destruction in power systems in Hawaii, and damaged three satellites in orbit. The

idea of using nuclear warheads in space started to die down because of these adverse effects on friendly hardware. [8], [12]

The main objective of Project Bold Orion (rockets launched from a B-47 bomber, in 1959) was researching the feasibility of using an air-launched ballistic missile, but the project was extended to be a possible ASAT system. Its final test version proved the concept and approached within four miles of the Explorer VI satellite. The US Navy's Early Spring Project was proposed to mount a modified Sparrow air to air missile on a sub-launched ballistic missile (SLBM) which would climb to the target's orbital altitude, wait until the target entered the engagement zone, and then destroy it by means of a proximity fuse and a conventional warhead. Another Navy project Skipper intended to launch a modified Scout rocket from a ship or submarine as a kinetic kill ASAT weapon. The Skipper was different from most of the other projects because it would not use a nuclear warhead. Neither the Early Spring nor the Skipper project was able to come into development. [16]

The US Army, conducted tests using the Nike-Zeus missile system which was originally developed as part of an Anti-Ballistic Missile (ABM) system. The first successful US anti-satellite intercept took place on May 23, 1963 from Kwajalein Island in the Pacific Ocean. Throughout the duration of Project Mudflap, at least eight of the Nike Zeus ground-launched missiles were fired until 1966. The US Air Force deployed Thor rockets which were modified for the anti-satellite mission through Operation Dominic and which had a capability of carrying a 1.5 megaton yield nuclear warhead to a target up to 200 nautical miles high. The Dominic project conducted

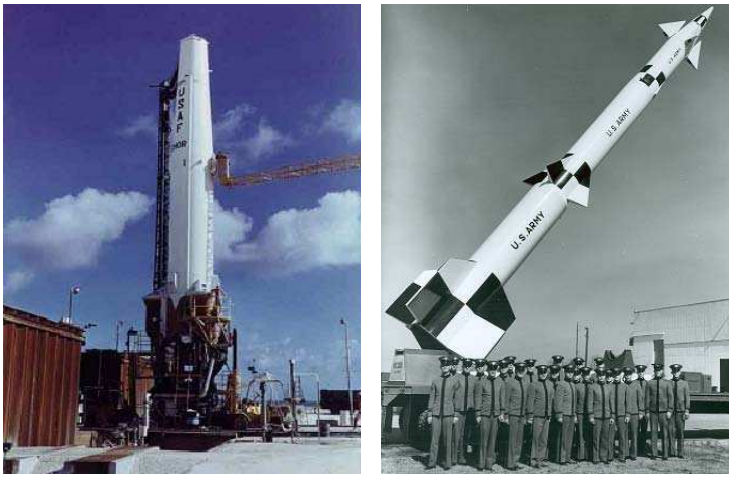

(a) (b)

Figure 2.1: Figure a, b, shows Thor and Nike-Zeus missiles respectively . [3], [19]

a series of high altitude nuclear tests in 1962 and later. The Thor system was tested at least 16 times from 1964 to 1970, prior to its retirement in 1976. Figure 2.1 shows the Nike-Zeus and Thor missiles used as ASAT weapons. [12], [19]

The concept of using Light Amplification by Stimulated Emission of Radiation (LASER) and Microwave Amplification by Stimulated Emission of Radiation technology (MASER) in an ASAT role of attacking the satellite's sensors and electronics goes back to the early 1960's. The United States was aware of the Soviet's improving development of particle beam ASAT capability, but emphasis remained on rocket powered interceptors. [12]

Russia's main ASAT system was the Co-Orbital ASAT system. The operation was based on a missile armed with conventional explosives. The 1400 kg ASAT interceptor was planned to be placed into a orbit close to the target satellite's orbit and then it maneuvered to get close to the target within one or two orbits. When

close enough, the ASAT, guided by its onboard radar, was directed toward the target, exploding and destroying the target using fragmentation effects. The project's initial testing phase was between 1963 and 1972. During this period approximately 20 launches, seven interceptions, and five detonations were executed. The initial tests confirmed that the system was operational from altitudes of 230 to 1,000 kilometers, and the system was declared operational. After signing the Anti-Ballistic Missile Treaty in 1972, the Soviets temporarily ceased tests, but in 1976 testing of the Co-Orbital system resumed. They have extended the operational altitude range between 160 km and 1600 km, minimized the attack time to a single orbit and started testing optical and infrared sensors in addition to onboard radar. Testing of the Soviet Co-Orbital ASAT weapon continued from 1978 to 1982, with approximately one intercept per year. Although it has not been tested for many years, the system is thought to be currently operational. [8]

The Air Force ASAT program, Miniature Homing Vehicle (MHV), was first mentioned in the magazine "Aviation Week & Space Technology" in March 1975. The MHV was a kinetic energy weapon launched from an F-15 and guided to its target by an infrared sensor mounted in its nose. This weapon was composed of a small two stage rocket and a Miniature Homing Vehicle (MHV) which would destroy its target by direct impact at high speed. Launching from the F-15 had the advantage of being able to bring MHV under the ground track of its target, as opposed to a ground-based system, which must wait for a target to overfly its launch site. After a long period of development, the MHV was finally tested against a defunct Army

Figure 2.2: Miniature Homing Vehicle launched from F-15. [12]

communications satellite in 1985, successfully destroying the target. The picture at Figure 2.2 was taken during one of the MHV tests. [12]

After high definition imagery from satellites in low Earth became very accessible, the US reinvigorated its effort to find a way to neutralize hostile satellites. The US Army's Kinetic Energy Anti-Satellite (KE ASAT) program started in 1989 and was to provide the United States with the capability to destroy hostile satellites. The Kinetic Kill Vehicle (KKV) would be launched by rocket booster to strike and destroy hostile satellites. An ASAT site would be located in the western United States or Pacific Ocean area. The KE ASAT would be launched when the target approached the firing zone. Then the KKV would separate from the rocket booster and make course corrections enabling it to strike the satellite and disable it with its unique debris mitigation device. After this the KKV would re-enter the atmosphere and burn up. The KKV already had been designed, developed, integrated, and ground-tested

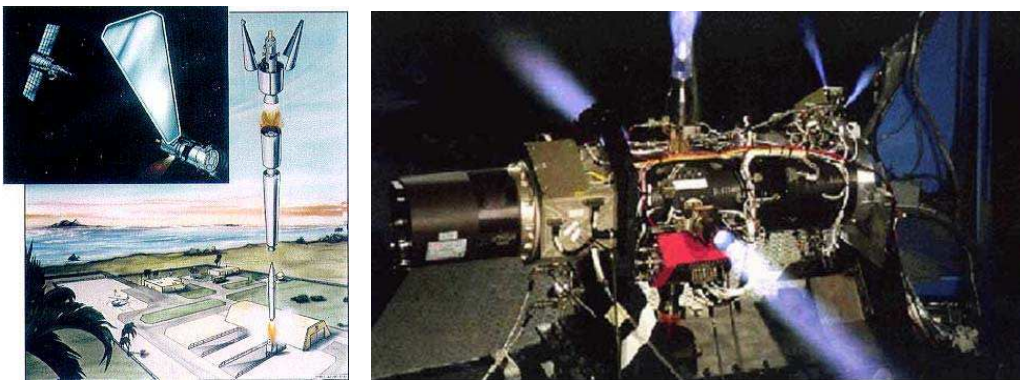

(a) (b)

Figure 2.3: Kinetic Energy ASAT. [12]

successfully and was supposed to have become mission capabile by 2000. Figure 2.3 depicts the KE ASAT. [12]

Both kinetic-kill and laser ASATs have relative advantages and disadvantages. Kinetic-kill vehicle systems provide easily verifiable destruction of a satellite and are independent of weather. Ground-based lasers, while susceptible to adverse weather, generate less space debris and also allow for a covert satellite strike. The US directed-energy ASAT system centered on the Mid-Infrared Advanced Chemical Laser (MIRACL) which was developed largely in 1989 and 1990. The MIRACL was the first megawatt-class, continuous wave, chemical laser built in the world. The US Air Force conducted a test of MIRACL in 1997. The laser was directed toward a satellite orbiting 420 km above the Earth. The MIRACL laser apparently had technical difficulties, but the results of the test were amazing. A lower-power (30-watt) laser, was used for alignment of the system and tracking of the satellite, but it was observed that this lower-power laser was powerful enough to blind the satellite temporarily, although it could not destroy the sensor. In the 1990's the Soviets also developed an

anti-satellite laser system, and their system was considered as a threat to satellites and ballistic missiles. [12]

Directed Energy Weapons include laser, high-power radio frequency, and particle beam technologies. A particle beam weapon proposes to accelerate charged particles to very high velocities. High-energy particle beams will produce high surface temperatures that can burn out the satellite electronics, produce high surface currents that will disrupt sensitive electronics, or produce ions, electrically charged particles that will disrupt satellite electronics via radiation effects. On-the-other-hand, it would be difficult and expensive to place particle beam weapons in orbit. Many tons of material must be lifted and a complex device must be constructed under free-fall conditions. Electronic signal manipulation is another major class of ASAT weapons effort. The signal to the satellite can be disrupted with a very high, electronic-competing signal. Traditional satellite components are also becoming smaller and lighter. This may eventually permit the launch of parasitic microsatellites which can maneuver close enough to the target satellite to disrupt or destroy it. In recent days, the US has begun working on several systems including the Experimental Spacecraft System (XSS-11), the Near-Field Infrared Experiment (NFIRE), and the Space-based Interceptor (SBI) programs. [12]

China's ASAT test of 11 January is the sort of capability available to any country which has IRBMs or satellite launch vehicles and a long-range radar system, such as Japan, India, Pakistan, Iran, and even North Korea. Many countries now use space systems for military and intelligence purposes. In addition to the US and

Russia, for example, several European countries, Israel, India and Japan also maintain reconnaissance satellites in LEO, and these are all vulnerable to ASAT missiles. [12], [17],

2.2 Space Surveillance

2.2.1 Overview. For the most part, the initial intent of space surveillance sensors was to provide warning of a strategic missile attack. However, the rising number of satellites created a requirement to watch all satellites during their lifecycle, including launch and decay, in order not to confuse them with hostile missiles. Eventually, the space surveillance operations started to separate from missile defense operations with the increase of the military importance of space.

Both optical and radar systems are used as satellite tracking systems and they mostly use the latest and most expensive sensor technologies. Most optical sensors are dependent on reflected sunlight or emitted infrared energy to track a satellite. On-the-other-hand, active optical sensors, illuminating a target with coherent laser radiation are being used in some recent applications. By illuminating a target with laser radiation, these systems can image satellites that are not reflecting sunlight. Active illumination also provides measurement of the range to the target. Ground-based radar systems have been used since the late 1950s for space surveillance applications. Radars have the advantage of being able to track the target any time and uninterruptedly during cloudy conditions as compared to optical sensors. Today, using the advanced technology of large phased array radars (LPAR), a great variety of opera-

tions including satellite tracking, missile early warning, and guiding interceptors as apart of ABM systems can be accomplished.

2.2.2 United States Space Surveillance Network. One part of United States Space Command (USSPACECOM)'s mission is to detect, track, catalog and identify man-made objects orbiting Earth. These include active and defunct satellites, rocket bodies, and debris. As described by the USSPACECOM itself, space surveillance accomplishes the following:

- "Predict when and where a decaying space object will re-enter the Earth's atmosphere;
- Prevent a returning space object, which to radar looks like a missile, from triggering a false alarm in missile-attack warning sensors of the US and other countries;
- Chart the present position of space objects and plot their anticipated orbital paths;
- Detect new man-made objects in space;
- Produce a running catalog of man-made space objects;
- Determine which country owns a re-entering space object;
- Inform NASA whether or not objects may interfere with the space shuttle and Russian Mir space station orbits. [1]"

The Space Surveillance Network (SSN) accomplishes these efforts via US Army, Navy and Air Force operated ground-based radars and optical sensors at 25 sites worldwide. The SSN started tracking Sputnik I and is still observing and tracking space objects.

The SSN has tracked more than 24,500 space objects orbiting Earth since the launch of Sputnik I in 1957. Most of these objects have decayed entering the Earth's

atmosphere, and the SSN tracks more than 8,000 orbiting objects now. Beside satellites, rocket body pieces of 10 pounds and space objects as small as 10 centimeters in diameter can be tracked by SSN. The number of operational satellites is approximately seven percent of the total number of 8,000; all of the other objects are debris. The SSN predicts the space objects' orbits and checks the objects at an instant rather then continuously following them because of the limited number of sensors and other limited capabilities of the network. The US SSN radar sensors and their field of view at 500 km altitude is pictured in Figure 2.4.

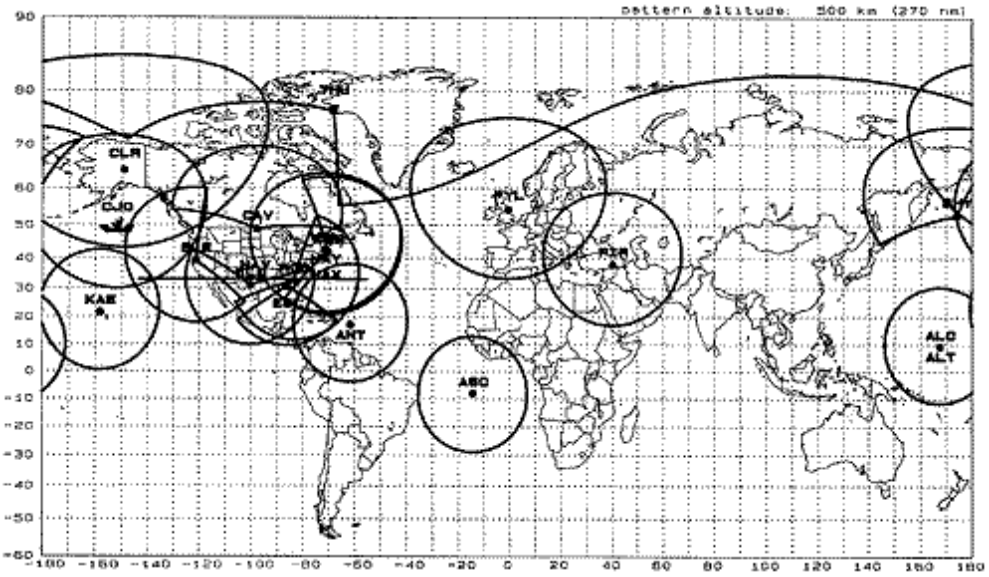

Figure 2.4: Space Surveillance Network Radar Sensors and their field of view at 500 km Altitude. [11]

The SSN consists of the following:

Phased-array radars have no moving mechanical parts, and the radar energy is directed electronically. Using this advantage, these radars can track multiple satellites simultaneously and scan large areas of space in a very short time.

For instance, the AN/FPS-85 phased-array radar at Eglin AFB in Florida is composed of almost 6,000 transmitter antennas and 20,000 receiver antennas and can track objects from just above the horizon to very close to the zenith over an azimuth of 120 degrees. It can track space objects up to 40,000 kilometers in range.

Conventional radars composed of tracking and immobile antennas which operate in bistatic mode. Bistatic mode means one antenna transmits a pulse and another receives the reflected signals. The Naval Space Surveillance System (NAVSPASUR), operating with conventional radars, is a network of three transmitting and six receiving radars providing continuous observation and detection of space objects crossing the continental United States.

Ground-Based Electro-Optical Deep Space Surveillance System (GEODSS) consists of three operational sites at Socorro, New Mexico; Maui, Hawaii; and Diego Garcia, British Indian Ocean Territories. GEODSS combines the functions of telescope, low-light-level television and computers to perform the surveillance missions. Each site has three telescopes. An example complex is seen in Figure 2.6. The system only operates at night but has the capability to detect objects 10,000 times dimmer than the human eye can detect. Since it is an optical system, it is adversely effected by cloud cover and local weather conditions. GEODSS can track objects as small as a basketball at a distance of more than 20,000 miles in space. It has a critical role of tracking deep space objects including geostationary satellites. The location of the GEODSS sites

with optical track capability and their coverage at 500 kilometers can be seen at Figure 2.5.

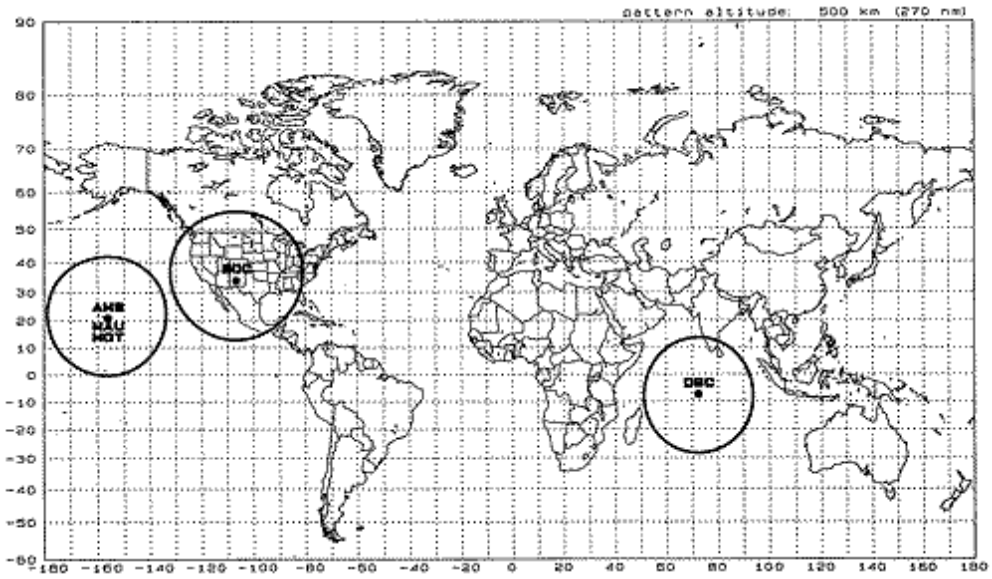

Figure 2.5: Locations of GEODSS Sensors and their field of view at 500 km Altitude. [11]

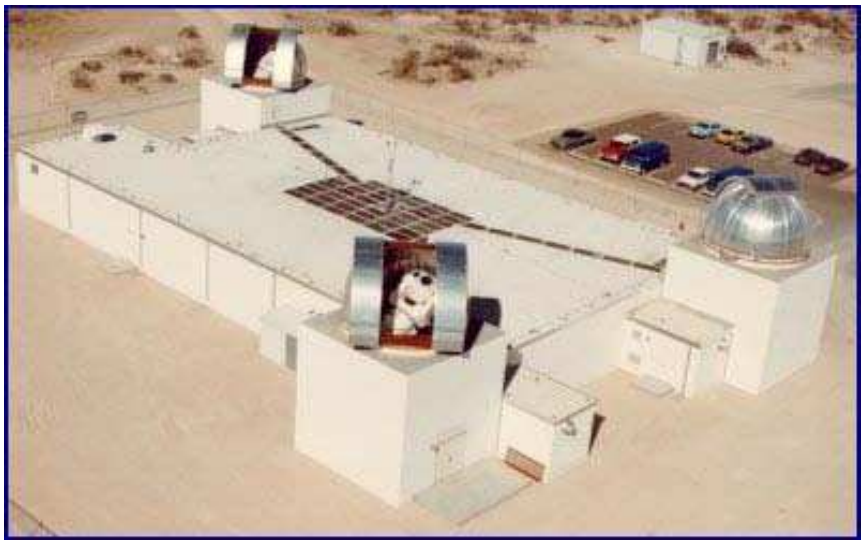

Figure 2.6: GEODSS Site. (Reference: space.kursknet.ru)

All these different types of sensors, located at different SSN sites such as Maui, Eglin, Thule, and Diego Garcia collect up to 80,000 satellite observations each day.

Each station transmits its data directly to USSPACECOM's Space Control Center (SCC) by means of satellite, ground wire, microwave, and phone. The SCC in Cheyenne Mountain Air Station is the nucleus of the SSN where the enormous amount of data flows. The Cheyenne Mountain command center is seen in Figure 2.7. The SCC uses computer aided systems to process SSN information and accomplish the space surveillance and space control missions. The NAVSPACECOM is the site for the Alternate SCC (ASCC). [11], [17].

Figure 2.7: Cheyenne Mountain Command Center. [13]

2.2.3 Russian and European Space Surveillance Network. The Russian space surveillance system uses an the early-warning radar network and is operated by the space-surveillance division of the 3rd Army. The network also includes the Krona system at Zelenchukskaya in the North Caucasus and Nakhodka on the Far East. The main optical observation station that monitors objects on high-altitude orbits is

called Okno and is located in Nurek, Tajikistan. Okno can detect objects at altitudes of up to 40,000 km.

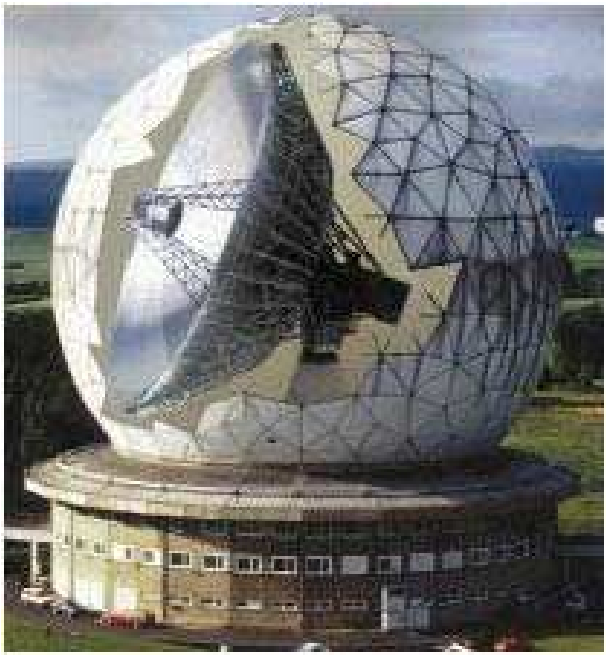

Figure 2.8: The FGAN Tracking and Imaging Radar (TIRA) at Wachtberg, Germany. [14]

Although ESA and European countries with space monitoring capabilities are strongly dependent on initial object and orbit information provided by USSPACECOM, European countries have the capability to track the Earth orbital environment up to and beyond GEO altitudes. Main coordination of the systems is done by the European Space Agency. The ESA Space Debris Telescope, the French ROSACE/-TAROT system, and the UK PIMS sensors can detect GEO objects well below the stated USSPACECOM size threshold of 1 m in diameter. The GRAVES receiver at Apt, France; the FGAN Tracking & Imaging Radar (TIRA) at Wachtberg, Germany (shown at Figure 2.8); Phased-array surveillance radar and tracking radars at Fyling-

dales, UK; Norwegian Globus II radar; British Radar at Fylingdales, UK; the French GRAVES system; the Chilbolton radar located in Winchester,UK and the European Incoherent Scatter Radar are some of the powerful radars that are used for space surveillance and early warning operations. [14]

2.3 Ballistic Missile Defense Platforms and Sensors

For an effective ballistic missile defence, a group of sensors which are a combination of land, sea or space based sensors should be incorporated to detect and track a threat missile through its trajectory. Only a worldwide sensor coverage network can track a missile during all boost, midcourse and terminal phases.

Defense Support Program (DSP) Satellites are orbiting the earth approximately 35,780 kilometers over the equator in a geosynchronous orbit. The system provides global coverage for early warning, tracking and identification using infrared sensors to detect heat from missile and booster plumes against the Earth's background. Recently, in addition to their primary mission of ballistic missile defense, DSP satellites' infrared sensors started to be used in an early warning system for natural disasters like volcanic eruptions and forest fires.

Space Based Infrared System (SBIRS) program is the follow-on capability to the Defense Support Program (DSP). DSP has has been used for more than 30 years as an early warning systems for ballistic missile launches. Now the goal of the US is to provide transition from DSP to SBIRS without any gap in the ABM defense system. The SBIRS program currently includes two Geosyn-

chronous Earth Orbit (GEO) satellites, two Highly Elliptical Orbit (HEO) payloads installed on GEO satellites, and ground systems deployed around the world. SBIRS provides early warning of ballistic missile attacks and high precision information for ABM systems to intercept and destroy threat missiles. The system is currently under development by the US Air Force and a proposed future constellation is pictured in Figure 2.9.

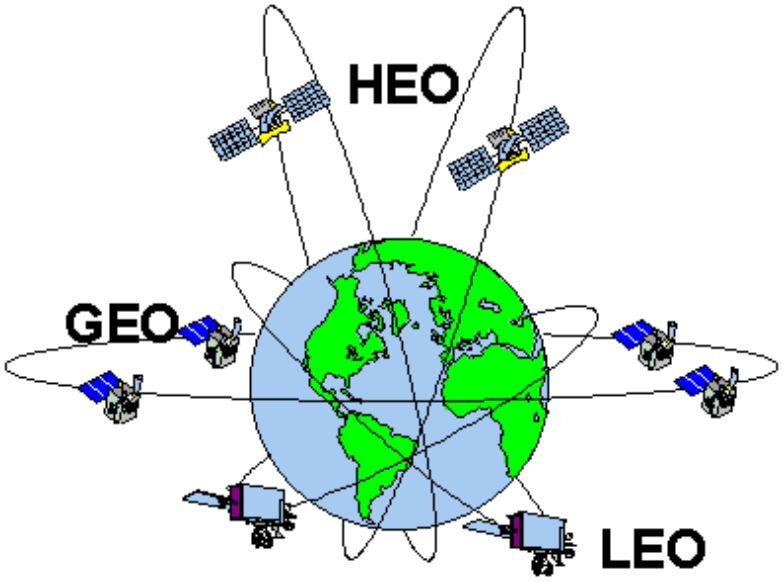

Figure 2.9: Proposed SBIRS space segment constellation. [11]

Early Warning Radars (EWR) are aiming to determine the final destination of threat missiles more precisely. Ground-based radars located in California, Alaska and overseas are being upgraded by the US in order to be used more effectively with the developing ballistic missile defense system.

X-Band Radars are capable of searching, detecting and tracking missiles. They can also distinguish between warheads and decoys. One of the latest version of

X-Band radars is currently being constructed by the US Missile Defense Agency. It is an X-band radar mounted on a moveable semi-submersible oil drilling platform. Sea based X-band radar, shown in Figure 2.10, will be home-ported in Adak, Alaska and will increase the overall success of ballistic missile defense systems with its capability to move throughout ocean areas for operations and testing.

Figure 2.10: Sea based X-band radar. [1]

THAAD Radars are the main sensors of the Terminal High Altitude Area Defense (THAAD) system. This valuable subsystem of the BMD system is rapidly transportable and forward-deployable. The upgraded version will have the capability to intercept and destroy ballistic missiles inside or outside the atmosphere while they are in their final, or terminal phase of flight.

SPY-1 Radar is mounted on Aegis cruisers and destroyers and a part of the BMD Agency's sea based ABM system. Aegis Destroyers with S-Band phased array

SPY-1 radars detect and track Intercontinental Ballistic Missiles and report track data to other systems and sites of BMD sysytem.

Forward Deployable Radars (FDR) can even be air transportable and provide additional sensor capability for tracking hostile missiles. Forward Deployable Radars are intended to be placed at sites close to the launch area of ballistic missiles where they can obtain more accurate tracking data very early and transfer this data to friendly interceptors providing additional time for more successful defensive intercepts. [1]

2.4 Previous Research

The Space-Based Visible Program was aiming to accomplish the technology demonstration of space based space surveillance with the Midcourse Space Experiment satellite. The satellite was launched in 1996 into a near sun-synchronous LEO orbit with an onboard visible-band electro-optical camera designed at Lincoln Laboratory. In 1997, technology demonstration was successfully achieved by gathering optical information on various space objects. Then, the space-based visible sensor associated with the program started to be used as a part of US Space Surveillance Network with a proved capability at least as accurate as GEODSS sensors of the network. [7]

In a paper, C. B. Chang examined the problem of ballistic trajectory estimation with angle-only measurements. Earth gravity was assumed as the predominant and only force on the long range ballistic missile trajectory. An iterative least squares algorithm was used to determine the state of the trajectory with angle only measure-

ments. Both ground-based and space-based sensors were considered. The estimation algorithm described in this paper is emphasized as applicable to state estimation problems. [5]

In the paper "Ballistic Missile Track Initiation From Satellite Observations", written by Murali Yeddanapudi, Yaakov Bar-Shalom, Krishna R. Pattipati, Somnath Deb, an algorithm is presented to track a ballistic missile in the initial phase, out of atmosphere, using line-of-sight measurements from one or more moving sensors, typically mounted on satellites. Results of the estimation problem were considered as non-satisfactory because of the poor target motion capability when using the Gauss-Newton iterative least squares minimization algorithm for estimating the state of a nonlinear deterministic system with nonlinear noisy measurements. The major problem with this approach was caused by strong dependence on initial guess. A more sophisticated Levenberg-Marquardt method was used in place of the simpler Gauss-Newton algorithm and robust new methods for obtaining the initial guess in both single and multiple satellite scenarios were developed. The sensor was considered to be both passive and active. Monte Carlo simulation studies on some typical scenarios were performed, and the results indicate that the proposed estimators are efficient. [15]

Most of the studies about ASAT systems and anti-ASAT systems are classified or have a restricted distribution. As an example, the AFIT thesis titled 'Protection of a High Valued Space Asset' describes a current gap at situational space awareness and offers an onboard sensor system as a preferred solution. Candidate active and passive

sensors are revealed. As a short term protection solution for space based high-valued assets, employing optical sensors for each payload is recommended. Restrictions on this research prevent its exact recommendations from being published. However, just knowing the type of recommended sensor helped to focus this thesis. [4]

2.5 Chapter Summary

ASAT systems have been commonly developed, tested, and prepared for use since 1950's. The technology developed rapidly after the first space launches. With the recent Chinese test, it is proven one more time that KE ASAT weapons can easily be used to threaten LEO satellites. Improved applications of rocket technology, guidance systems and more effective warheads make the space-based assets more vulnerable. On-the-other-hand, space surveillance and ballistic missile defense efforts, briefly described through the chapter, shows that precautions against ASAT weapons should be composed of worldwide network of systems, including highly accurate sensors. Previous researches emphasize that even the US has some gaps in defending their space assets against ASATs. Also, there are a lot of countries that have satellites but don't have space surveillance sensors. It is obvious that, if the decision is based upon the information coming from external data sources, on most occasions there will not be enough time to maneuver the satellite defensively. Finally, the idea of having a sensor onboard the space asset with an early warning capability has matured. If the satellite can watch the earth, especially the suspicious areas and detect and track

a possible incoming ballistic-missile, it might have enough time to defeat the missile and survive.

III. Methodology

In this section, the methodology of estimating the ASAT missile's trajectory based on a space-based optical sensor's measurements will be analyzed. Initially, the orbit of the FY-1C satellite and the trajectory of the ASAT missile were created using two body dynamics. The state vectors including position and velocity for each of them were created throughout the flight time of the ASAT missile at different time steps. These data assumed to be true and true observations were generated using these state vectors. Then, some noise was added to those observations and simulated real world observations were computed. The least squares estimation filter which was gathering these observation data as input and generating estimated state of the ASAT missile at epoch time, was set up. Finally, the most probable converged estimated state at epoch time was propagated in time and the position of the ASAT missile with respect to the target at the time of impact was found. The flow of this process is explained in Figure 3.1.

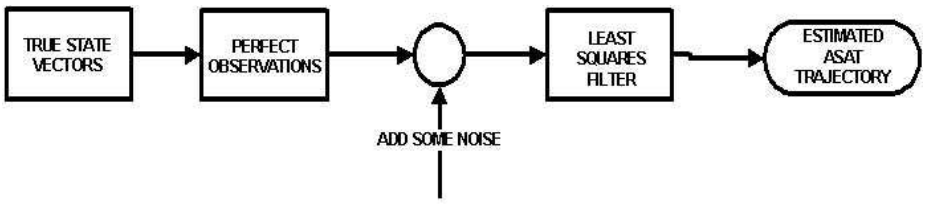

Figure 3.1: Analysis Flow Diagram.

3.1 Assumptions

- In the *Principia* Newton formulated the law of gravity beside his three laws of motion. The law of gravity is expressed in Equation 3.1, where G is the

universal gravitational constant, F is the gravitational force on mass m caused by mass M and $\mathbf{r}$ is the vector pointing from M to m. Any set of two bodies attract each other with a force proportional to the product of their masses and inversely proportional to the square of the distance between them. This principal is the basic law for the motion of the satellites and planets.

$$F_{GRAVITY} = -\frac{GMm}{r^2}\frac{\mathbf{r}}{r} \tag{3.1}$$

However, when the relative motion of two bodies in real world is considered, it has been observed and proved that some perturbations are involved in to the dynamics. A perturbation can generally be described as a deviation from the expected behavior. Some forces caused by atmospheric drag and lift, thrust, solar radiation, magnetic and relativistic effects, the Earth's and the Moon's non-perfect-spherical shapes, and forces due to additional space objects all cause deviations during the relative motion of the two bodies. The two-body problem was described to simplify the equation of motion for only two bodies with assumptions that the masses of the bodies can be concentrated at their centers, and there is not any force other than gravitational force acting on the system along the line joining the centers of the bodies. To accomplish the initial study about this topic, the two-body equation of motion (EOM) is applied to the motion of the satellite and the ASAT weapon targeting the satellite. The other

perturbations affecting their relative motion are neglected and assumed to be easily added in future studies. [18]

- The simulated Chinese ASAT weapon is assumed to be a modified but unguided ballistic missile. The missile does not make any correction on its track to the targeted satellite.
- The optical sensor on the satellite can establish line of sight measurements with an accuracy of up to 1/1000 *Arcseconds*.
- The missile can be tracked throughout its entire flight path including launch and impact. The atmospheric affects on the optical observations like reflection, refraction or the attenuation of the light are neglected.
- Since the curvature of the earth is not considered in the calculations, it is assumed that the line of sight between the sensor and the ASAT missile is not obstructed by the earth.
- As described in the two-body problem, neither the satellite's nor the ASAT missile's orbits are influenced by atmospheric affects. The trajectory of the ASAT missile is assumed to be always exo-atmospheric.
- It is supposed that the satellite is able to calculate its position and velocity vectors with respect to the geocentric equatorial coordinate system at every thousandth of a second and its calculations are assumed to be free of error.

3.2 Scenario

The actual Chinese ASAT test conducted on January 2007 is represented in the scenario. The Chinese defunct weather satellite FENG YUN-1C's orbital parameters were available as open public information. Using those data the state vector of the satellite $X_{sat}= [x, y, z, V_x, V_y, V_z]^T$, composed of its position and the velocity vectors with respect to the inertial frame, were created. The state vector of the satellite at the impact time, 5:28 p.m. EST on January 11, 2007, was also determined. Since we have the information about the location of the launch area, which was the Chinese Xichang space complex, we knew the start and the end points of the ASAT missile's trajectory. Applying approximate launch parameters for an IRBM which is capable of this mission, and the location of the two end-points, the trajectory which will best fit in these data was created. In general there would be two possible impact points in the missile trajectory but the problem was set up such that the impact occurs at the missile's apogee. In these calculations, the closest interception between two orbital tracks is selected as the impact point and the state vector of the ASAT missile $X_{ref}= [x, y, z, V_x, V_y, V_z]^T$ was created. The state vectors for both the satellite and the ASAT missile were generated for different time intervals throughout the entire missile flight time of approximately 8 *minutes*. These data or the software program used to create these data are not demonstrated in this thesis because they are straightforward and simple to reproduce. These vectors were assumed to be perfect and used to calculate the simulated observations achieved by the onboard sensor.

The scenario is such that we assume the sensor on the satellite was tracking the earth continuously and had the locations of the possible threat launch sites stored in its database. Whenever it caught a threat it would begin to make observations and calculate the position of the missile at each observation time step. After having enough data it would calculate the estimated track of the ASAT missile and compare it with its own orbit in order to estimate a possible intersection. The number of observations required to make an estimate depends on the accuracy of the sensor and the time intervals between the observations. Once the sensor obtained enough observations it would propagate the missile trajectory and calculate the standard deviation of the miss distance between the two orbits at the possible intersection time. Being aware of this possible intersection error ellipsoid would provide the satellite the chance to make a last ditch manoeuver to defeat the ASAT missile.

3.3 Dynamics

As mentioned in the assumptions section, in this research numerical integrations of the two-body problem were used to calculate the state vectors of the targeted satellite and the ASAT missile. Initially, the state vectors, composed of position and velocity vectors with respect to the geocentric equatorial coordinate system, were created and they were assumed to be the "*truth*." Then simulated observation measurements were created based on this true data and some statistically relevant additional error. A brief explanation of the two-body problem is considered to be helpful.

The two-body problem is a result of Newton's second law, and two assumptions that (1) the bodies can be represented as point masses and (2) there is no other force acting on them other than the gravitational force. To be able to describe the relative motion of the two bodies, an inertial frame should be described. Newton described this inertial frame as *"in its own nature, without relation to anything external, remains always similar and immovable."* There is an ongoing discussion on his inertial frame definition but it can be assumed as *almost inertial* and then proceed to explain the two-body problem. [18]

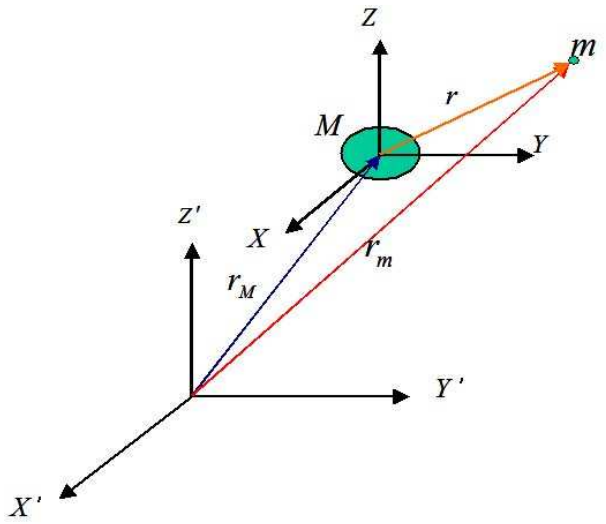

Figure 3.2: Relative Motion of Two Bodies.

In the book named Fundamentals of Astrodynamics [18] two bodies with masses M and m are considered and pictured as in Figure 3.2. Their position is defined with respect to an inertial frame (X', Y', Z') and a secondary non rotating reference frame (X, Y, Z), which is parallel to the inertial frame and originated at the center of mass M. The vector r is defined as $r = r_m - r_M$.

Applying Newton's second law in the inertial frame the dynamics equations become

$$m\ddot{r}_m = -\frac{GMm}{r^2}\,\frac{\mathbf{r}}{r} \tag{3.2}$$

$$M\ddot{r}_M = \frac{GMm}{r^2}\,\frac{\mathbf{r}}{r} \tag{3.3}$$

These equations are simplified and written as

$$\ddot{r}_m = -\frac{GM}{r^3}\,\mathbf{r} \tag{3.4}$$

$$\ddot{r}_M = \frac{Gm}{r^3}\,\mathbf{r} \tag{3.5}$$

Subtracting Equation (3.5) from Equation (3.4) the vector differential equation of the relative motion for the two-body problem is obtained as

$$\ddot{r} = -\frac{G(M+m)}{r^3}\,\mathbf{r} \tag{3.6}$$

When the situation in which a smaller object like an artificial satellite or a ballistic missile orbiting a planet is considered, the mass of the orbiting m will be very small when compared to the central body M, so it can be assumed that

$$G(M+m) \approx GM \tag{3.7}$$

Finally, when the gravitational parameter $\mu \equiv GM$ is substituted in Equation (3.6), the convenient form of the two-body equation of motion is obtained in Equation (3.8).

$$\ddot{r} \; + \; \frac{\mu}{r^3} \, \mathbf{r} \; = \; 0 \tag{3.8}$$

3.4 Filter

3.4.1 Least Squares Estimation. In the two-body problem, six classical orbital elements define the orbit. There should be at least six observations in order to calculate these six orbital elements. Although it can be assumed that the dynamics are perfect, the observations include errors and in most applications there are more observations than six. A German mathematics student Carl Freidrich Gauss discovered the Principal of Maximum Likelihood and the Least Squares method, solved these orbit determination problems and succeeded to determine the orbit of asteroid Ceres. Ceres was first observed by Piazzi but lost after a few observations. Gauss calculated the orbit that passes as close as possible to all observation points obtained by Piazzi and the lost asteroid Ceres was discovered using the orbit determined with least squares estimation. [20]

3.4.1.1 The Principle of Maximum Likelihood. Initially, it can be assumed that in order to find the wanted value of x_0, N independent measurements of x_i were obtained using different equipment, and each data had standard deviation

σ_i. The joint probability can be calculated as the product of the individual Gaussian distributions.

$$P(x_1, x_2, ...x_N) = (2\pi)^{\frac{-N}{2}} \left[\prod_{i=1}^{N} \sigma_i^{-1}\right] \times \exp(-\sum_{i=1}^{N} \frac{(x_i - x_0)^2}{2\sigma_i^2}) \tag{3.9}$$

Since the true value x_0 in Equation (3.9) is always unobtainable, an estimate $\bar{x}$ of the wanted true x_0 value is replaced for it.

$$P(x_1, x_2, ...x_N) = (2\pi)^{\frac{-N}{2}} \left[\prod_{i=1}^{N} \sigma_i^{-1}\right] \times \exp(-\sum_{i=1}^{N} \frac{(x_i - \bar{x})^2}{2\sigma_i^2}) \tag{3.10}$$

The value of $\bar{x}$ which is closest to the truth can be obtained by maximizing the probability in Equation (3.10) with respect to $\bar{x}$. And the maximum of that equation can be obtained when the argument of the exponential is minimized.

$$\frac{d}{d\bar{x}} \sum_{i=1}^{N} \frac{(x_i - \bar{x})^2}{2\sigma_i^2} = 0 \tag{3.11}$$

This step of the principal is alternately named as *the method of least squares*. [20]

3.4.1.2 Linearization of Dynamics . The equations of motion used in this thesis are especially based on the two-body dynamics. State vectors x of a satellite and an ASAT missile were created and estimated. The state vectors of the dynamic system were composed of position and velocity vectors. As Wiesel describes

in his text, the equations of motion determine the evaluation of the state vector with time as the differential equations

$$\frac{dx}{dt} = \mathbf{g}(x, t) \tag{3.12}$$

or the closed-form solution can be written as relating the actual state to the initial state and time.

$$x(t) = h(x(t_0), t) \tag{3.13}$$

Both of these equations can be used to calculate the changes of the true state x_0, the estimated state $\bar{x}$, and the nearby trajectories. It can be assumed that the estimate of the true trajectory will be very close to the true trajectory and express their relation as $x = x_0 + \delta x$. Substituting this expression into the equations of motion (3.12), expanding $\mathbf{g}$ in a Taylor's series, and ignoring second and higher order terms the equation becomes

$$\begin{aligned} \frac{dx}{dt} &= \mathbf{g}(x_0 + \delta x, t) \\ &\approx \mathbf{g}(x_0, t) + \nabla_x \mathbf{g}(x_0, t)\delta x + O(2) \end{aligned} \tag{3.14}$$

Using Equation (3.14) *the Equations of Variation* are expressed as

$$\frac{d}{dt}\,\delta x \;=\; A(t)\,\delta x \tag{3.15}$$

where

$$A(t) \;=\; \nabla_x\,\mathbf{g}_{x_0(t)} \tag{3.16}$$

Recalling the fact that equations of variations are linear ordinary differential equations, Wiesel derived and defined the *State Transition Matrix* Φ as

$$\delta x(t) \;=\; \Phi(t,t_0)\,\delta x(t_0) \tag{3.17}$$

where Φ satisfies the equation

$$\frac{d}{dt}\,\Phi(t,t_0) \;=\; A(t)\,\Phi(t,t_0) \tag{3.18}$$

with initial conditions

$$\Phi(t_0,t_0) \;=\; I \tag{3.19}$$

In Equation (3.19) the term I represents the identity matrix. In linear systems Φ is used to propagate the state in time; however, in nonlinear systems Φ matrix propagates the small variation of the state δx in time. Whenever the equations of

motion are available in closed form, the state transition matrix for each time step can be obtained by numerical integration. [20]

3.4.1.3 Linear Least Squares. Linear least squares method is used to estimate the state of a linear dynamical system at an epoch time t_0 with using the observations $z_i(t_i)$ taken at time t_i. Each observation vector $z_i(t_i)$ is assumed to be independent, unbiased and has an associated instrumental covariance Q_i. If observation data is linearly related to the system state at the measurement time, observation relation can be expressed as

$$z_i(t_i) = H_i \; x(t_i) \; + \; e_i \tag{3.20}$$

in which e_i is the true error of the observation. If we insert the system dynamics into this relation and substitute the definition $T_i \; \equiv \; H_i \; \Phi(t_i, t_0)$ we get a more compact observation relation.

$$\begin{aligned} z_i(t_i) \;\; &= \;\; H_i \; \Phi(t_i, t_0) x(t_0) \; + \; e_i \\ z_i(t_i) \;\; &= \;\; T_i x(t_0) \; + \; e_i \end{aligned} \tag{3.21}$$

Following the method in Wiesel's text, the total data vector z, the observation matrix T and the instrumental covariance matrix Q can be created

$$z \equiv \begin{bmatrix} z_1 \\ z_2 \\ \vdots \\ z_N \end{bmatrix} \tag{3.22}$$

$$T \equiv \begin{bmatrix} T_1 \\ T_2 \\ \vdots \\ T_N \end{bmatrix} = \begin{bmatrix} H_1\Phi(t_1, t_0) \\ H_2\Phi(t_2, t_0) \\ \vdots \\ H_N\Phi(t_N, t_0) \end{bmatrix} \tag{3.23}$$

$$Q \equiv \begin{bmatrix} Q_1 & 0 & \cdots & 0 \\ 0 & Q_2 & \cdots & 0 \\ \vdots & \vdots & \ddots & \vdots \\ 0 & 0 & \cdots & Q_N \end{bmatrix} \tag{3.24}$$

for N number of observations. And after some derivations Wiesel defines the estimate of the state vector $\bar{x}(t_0)$ and the covariance matrix $P_{\bar{x}(t_0)}$ at an epoch time. [20]

$$\bar{x}(t_0) = (T^T Q^{-1} T)^{-1} T^T Q^{-1} z \tag{3.25}$$

$$P_{\bar{x}(t_0)} = (T^T Q^{-1} T)^{-1} \tag{3.26}$$

3.4.1.4 Nonlinear Least Squares. Nonlinear least squares method is much more appropriate when solving the real world problems compared to the linear least squares, because in real world most of the dynamics and the observation relations are nonlinear. Also, the solution of the two-body problem, used in this thesis, is highly nonlinear. Linearization of these nonlinear system dynamics can be established with some assumptions. Again, following Wiesel's method, assuming system dynamics are available, they can be expressed in two forms as

$$\frac{dx}{dt} = f(x,t) \tag{3.27}$$

$$x(t) = h(x(t_0),t) \tag{3.28}$$

where Equation (3.27) represents the case when we have the equations of motion and Equation (3.28) is the explicit solution of the dynamics as a function of time and the initial conditions. Assuming that the dynamics are deterministic, linearization of the dynamics about a reference trajectory x_{ref}

$$\delta x(t) = \Phi(t,t_0)\ \delta x(t_0) \tag{3.29}$$

should be valid. The reference trajectory x_{ref} is expected to be close to the estimated trajectory $\bar{x}$ which is used instead of the unobtainable true trajectory x_0, and δx is expected to be small. The δx amount of changes will correct the reference trajectory x_{ref} and turn it into the closest estimate $\bar{x}$ of the true trajectory x_0.

The observations will be nonlinearly related to the current state at that time. This can be expressed as

$$z_i(t_i) \;=\; G(x(t_i), t_i) \tag{3.30}$$

where $z(t_i)$ are the measurements taken during the observation at time t_i. In real world applications all measurements include some error. If we were able to find a perfect instrument, it would observe the true state x_0 and generate the true observation data z_0. The vector of actual measurements with true error is defined as z and the imperfect observed state is called x. Assuming that true error in the data goes to zero when the error in the state approaches to zero, and also assuming that they are both small enough, the true error in the actual data becomes

$$e \;=\; z - z_0 \;=\; G(x,t) \;-\; G(x_0,t) \tag{3.31}$$

$$\;=\; G(x_0 + \delta x, t) - \; G(x_0, t) \tag{3.32}$$

$$\approx\; \frac{\delta G}{\delta x}\delta x(t) \tag{3.33}$$

where $x = x_0 + \delta x$, $e \approx r$ (in which r represents the *residuals*) and the matrix in the Equation (3.33) relates the errors in the state to the reference trajectory. The residuals can be represented as

$$r_i \;=\; z_i - G(x_{ref}(t_i), t_i) \tag{3.34}$$

Similar to the linear case, H matrix is for the nonlinear case is defined as

$$H_i = \frac{\delta G}{\delta x}\left(x_{ref}(t_i), t_i\right) \tag{3.35}$$

Using the fact that these residuals are linearly related to δx, which changes the reference trajectory to into an estimated trajectory, and δx propagates as shown in Equation (3.29), the residuals equation becomes

$$r_i \approx H_i \delta x(t_i) = H_i \Phi(t_i, t_0)\delta x(t_0) \tag{3.36}$$

$$= T_i \delta x(t_0) \tag{3.37}$$

Finally, the solution for the nonlinear least squares estimation can be written as

$$\delta x(t_0) = (T^T Q^{-1} T)^{-1} T^T Q^{-1} r \tag{3.38}$$

$$P_{\delta x} = (T^T Q^{-1} T)^{-1} \tag{3.39}$$

where δx is the small variances to the reference trajectory and $P_{\delta x}$ is the covariance matrix. The general form of the covariance matrix in Equation 3.39 is a symmetric

matrix

$$P = \begin{bmatrix} P_{11} & P_{12} & \cdots & P_{1N} \\ P_{12} & P_{22} & \cdots & P_{2N} \\ \vdots & \vdots & \ddots & \vdots \\ P_{1N} & P_{2N} & \cdots & P_{NN} \end{bmatrix} \tag{3.40}$$

where the diagonal components P_{ii} are the variances representing the σ_{ii}^2 values and the off diagonal components represent the covariances. In a special case where all the measurements are statistically independent of each other the covariance matrix becomes [20]

$$P = \begin{bmatrix} \sigma_1^2 & 0 & \cdots & 0 \\ 0 & \sigma_2^2 & \cdots & 0 \\ \vdots & \vdots & \ddots & \vdots \\ 0 & 0 & \cdots & \sigma_N^2 \end{bmatrix} \tag{3.41}$$

and as Wiesel explains [20], the estimated trajectory is determined as

$$\bar{x}(t_0) = x_{ref}(t_0) \; + \; \delta x(t_0) \tag{3.42}$$

3.4.2 Observation Geometry. The purpose of this thesis is to analyze whether only one optical sensor designated for self defense can estimate a threat's trajectory based only on its observed measurements. Although we don't have any real world data to be used as the observations, measurements including simulated errors were generated using the assumed true trajectories. As mentioned previously,

the orbit of the satellite and the trajectory of the ASAT missile were created via numerical integration of the equations of motion throughout the flight time of the missile. The state vectors composed of position (x, y, z) and velocity (V_x, V_y, V_z) vectors for each time interval t_i were generated. The initial conditions were selected to fit in the scenario and achieve the impact at the given time using the closest intersection point. In order to do the integration in $MATLAB$, the equations of motion were written in matrix form.

$$\dot{X} = B(X)X \tag{3.43}$$

$$\begin{bmatrix} \dot{x} \\ \dot{y} \\ \dot{z} \\ \ddot{x} \\ \ddot{y} \\ \ddot{z} \end{bmatrix} = \begin{bmatrix} V_x \\ V_y \\ V_z \\ -\mu x/r^3 \\ -\mu y/r^3 \\ -\mu z/r^3 \end{bmatrix} = \underbrace{\begin{bmatrix} 0 & 0 & 0 & 1 & 0 & 0 \\ 0 & 0 & 0 & 0 & 1 & 0 \\ 0 & 0 & 0 & 0 & 0 & 1 \\ -\mu/r^3 & 0 & 0 & 0 & 0 & 0 \\ 0 & -\mu/r^3 & 0 & 0 & 0 & 0 \\ 0 & 0 & -\mu/r^3 & 0 & 0 & 0 \end{bmatrix}}_{B} \begin{bmatrix} x \\ y \\ z \\ V_x \\ V_y \\ V_z \end{bmatrix} \tag{3.44}$$

The optical sensor on the satellite is assumed to be able to achieve a line of sight measurement to an incoming ASAT missile. The exact position of the satellite $\vec{r}_{sat}$ is gathered from the central computer of the payload and it assumed to be true for

the observation time t_i. Given that the sensor is aware of the possible ASAT missile launch locations and the approximate launch parameters of a possible incoming missile we can say that the sensor can calculate the approximate position of the ASAT missile $\vec{r}_{asat}$.

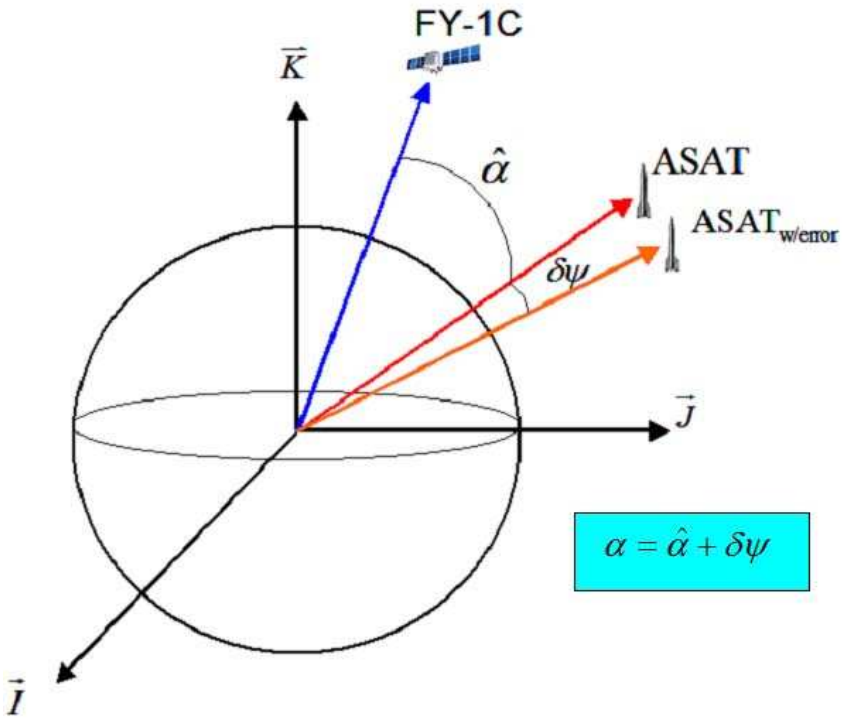

Figure 3.3: Observation Geometry.

The observation to be used is defined as the cosine of the angle between the position vectors of the satellite and the ASAT missile. If α is the observation angle, $z = \cos\alpha$ is the observation data measured by the sensor. This angle is defined as a theoretical angle to be used. Some other angles like the angle between the lines connecting the center of the earth, the satellite and the ASAT could also be used. The observation is not perfect and the observed angle α is related to the true angle

$\hat{\alpha}$ between the true position vectors as $\alpha = \hat{\alpha} + \delta\psi$, and represented in Figure 3.3. Then, the observation can be written as

$$z \;=\; \cos\alpha \;=\; \cos\left(\hat{\alpha} + \delta\psi\right) \tag{3.45}$$

where $\cos\hat{\alpha} \;=\; z_0$ is the true observation without error and $\delta\psi$ can be defined as the 1σ accuracy of the sensor; later this accuracy will be multiplied by a zero mean, discrete-time white Gaussian random number to generate error based on the fact that real instruments typically exhibit such statistics [9]. The error in the measurement can be expressed as

$$|\delta z| \;=\; |\cos\alpha - \cos\hat{\alpha}| = |\cos\left(\hat{\alpha} + \delta\psi\right) - \cos\hat{\alpha}| \tag{3.46}$$

and expanding the $\cos\left(\hat{\alpha} + \delta\psi\right)$ term the observation error becomes

$$|\delta z| \;=\; |\cos\hat{\alpha}\cos\delta\psi - \sin\hat{\alpha}\sin\delta\psi - \cos\hat{\alpha}| \tag{3.47}$$

Since the angle $\delta\psi$ is assumed to be small enough and with small angle assumptions

$$\begin{aligned} \cos\delta\psi &\approx 1 \\ \sin\delta\psi &\approx \delta\psi \end{aligned}$$

Equation (3.47) becomes

$$|\delta z| \;=\; |-\delta\psi \sin\hat{\alpha}| \tag{3.48}$$

Squaring both sides and substituting the $z_0 = \cos\hat{\alpha}$ we get

$$(\delta z)^2 \;=\; (\delta\psi)^2\,(1 - z_0^2) \tag{3.49}$$

Finally, applying estimation operator as described by Wiesel [20] the instrumental variance for each observation at time t_i can be obtained

$$(\sigma_z)^2 \;=\; (\sigma_\psi)^2\,(1 - z^2) = Q \tag{3.50}$$

in which σ_ψ is the variance of the sensor as given by the manufacturer or determined by experiment.

In this analysis initially, $z_0 = \cos\hat{\alpha}$ is calculated

$$\begin{aligned} z_0 \quad &= \quad \cos\hat{\alpha} \;=\; \frac{\vec{r}_{sat}\cdot\vec{r}_{asat}}{|\vec{r}_{sat}||\vec{r}_{asat}|} \\ &= \quad \frac{x_{sat}x_{asat} + y_{sat}y_{asat} + z_{sat}z_{asat}}{\sqrt{x_{sat}^2 + y_{sat}^2 + z_{sat}^2}\sqrt{x_{asat}^2 + y_{asat}^2 + z_{asat}^2}} \end{aligned} \tag{3.51}$$

and some error δz, as defined in the Equation (3.49), is added to each true observation in order to get the simulated real world measurements. In order to calculate erroneous simulated real world measurements z_i at each observation time t_i, the $\delta\psi$ term in

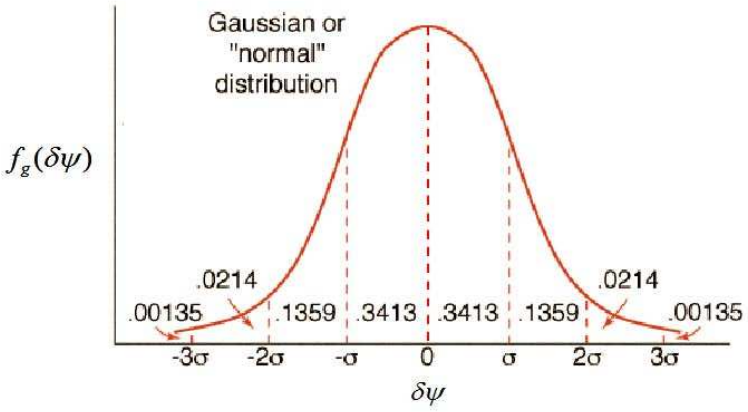

Figure 3.4: Gaussian Distribution of the Error. [2]

Equation (3.49) is multiplied with a random number, generated in $MATLAB$ using Gaussian distribution. Observation data for the entire flight time of the missile is obtained as

$$z \equiv \begin{bmatrix} z_1 \\ z_2 \\ \vdots \\ z_N \end{bmatrix} = \begin{bmatrix} z_{0_1} \\ z_{0_2} \\ \vdots \\ z_{0_N} \end{bmatrix} + \begin{bmatrix} c_1\sqrt{(1-z_{0_1}^2)} \\ c_2\sqrt{(1-z_{0_2}^2)} \\ \vdots \\ c_N\sqrt{(1-z_{0_N}^2)} \end{bmatrix} \tag{3.52}$$

where N is the total number of measurements and $c_1, c_2, ...c_N$ are the random numbers created based on Gaussian distribution with a mean of $\delta\psi$, which is shown in Figure 3.4. [2]

3.4.3 Filter Processing. The objective of this research is to determine the relative position of an unguided ballistic missile, modified as an ASAT weapon, with respect to the targeted satellite at the time of impact. This problem can be solved with a combination of estimator, dynamics model and data observations. The solution

of this problem is attempted to be achieved using a space-based onboard optical sensor, two-body dynamics, and least squares estimation. The nonlinear dynamical model to estimate the state of ASAT in this problem can be shown to be

$$X(t_i) = h(X(t_0), t_i) \tag{3.53}$$

where $X(t_0)$ is the state of the system at the epoch time t_0 and h is an analytic solution to the equations of motion. The observation relation wit the state is defined in

$$z(t_i) = G[X(t_i)] \ + \ v(t_i) \tag{3.54}$$

where $z(t_i)$ is the observation made at time t_i and $v(t_i)$ is an independent zero-mean discrete-time white Gaussian noise with a variance of Q. Further, in our case

$$z_0 = G(X_{ref}) = \cos\hat{\alpha} = \frac{x_{sat}x_{ref} + y_{sat}y_{ref} + z_{sat}z_{ref}}{\sqrt{x_{sat}^2 + y_{sat}^2 + z_{sat}^2}\sqrt{x_{ref}^2 + y_{ref}^2 + z_{ref}^2}} \tag{3.55}$$

and as defined in the nonlinear least squares section H_i is

$$H_i \ = \ \frac{\delta G}{\delta X} \ (X_{ref}(t_i), t_i) \tag{3.56}$$

If we define $r_{sat_i} = \sqrt{x_{sat_i}^2 + y_{sat_i}^2 + z_{sat_i}^2}$ and $r_{ref_i} = \sqrt{x_{ref_i}^2 + y_{ref_i}^2 + z_{ref_i}^2}$, the H matrix for each time t_i becomes

$$H = \left[(\frac{\delta G}{\delta x_{ref}})(\frac{\delta G}{\delta y_{ref}})(\frac{\delta G}{\delta z_{ref}})(\frac{\delta G}{\delta V_{x_{ref}}})(\frac{\delta G}{V_{y_{ref}}})(\frac{\delta G}{V_{z_{ref}}}) \right] \tag{3.57}$$

$$\begin{aligned}
H_{11} &= -\frac{x_{ref}(x_{sat}x_{ref} + y_{sat}y_{ref} + z_{sat}z_{ref})r_{sat}^2}{r_{sat}^3 r_{ref}^3} + \frac{x_{sat}}{r_{sat}r_{ref}} \\
H_{12} &= -\frac{y_{ref}(x_{sat}x_{ref} + y_{sat}y_{ref} + z_{sat}z_{ref})r_{sat}^2}{r_{sat}^3 r_{ref}^3} + \frac{y_{sat}}{r_{sat}r_{ref}} \\
H_{13} &= -\frac{z_{ref}(x_{sat}x_{ref} + y_{sat}y_{ref} + z_{sat}z_{ref})r_{sat}^2}{r_{sat}^3 r_{ref}^3} + \frac{z_{sat}}{r_{sat}r_{ref}} \\
H_{14} &= 0 \\
H_{15} &= 0 \\
H_{16} &= 0
\end{aligned} \tag{3.58}$$

In accordance with the algorithm for nonlinear least squares, as mentioned by Wiesel [20], the state vector should be propagated to the observation time t_i. In order to solve the state transition matrix Φ simultaneously with the state X their expression in the two-body equation of motion must be rearranged and written in matrix form to be numerically integrated in $MATLAB$. Recalling the two-body equation of motion

$$\ddot{r} \; + \; \frac{\mu}{r^3} \, \mathbf{r} \; = \; 0 \tag{3.59}$$

and the composition of the ASAT's state vector with respect to the geocentric equatorial coordinate frame

$$X = \begin{bmatrix} x \\ y \\ z \\ V_x \\ V_y \\ V_z \end{bmatrix} \tag{3.60}$$

and combining them in matrix form we get

$$\dot{X} \;=\; B(X)X \tag{3.61}$$

$$\begin{bmatrix} \dot{x} \\ \dot{y} \\ \dot{z} \\ \ddot{x} \\ \ddot{y} \\ \ddot{z} \end{bmatrix} = \begin{bmatrix} V_x \\ V_y \\ V_z \\ -\mu x/r^3 \\ -\mu y/r^3 \\ -\mu z/r^3 \end{bmatrix} = \underbrace{\begin{bmatrix} 0 & 0 & 0 & 1 & 0 & 0 \\ 0 & 0 & 0 & 0 & 1 & 0 \\ 0 & 0 & 0 & 0 & 0 & 1 \\ -\mu/r^3 & 0 & 0 & 0 & 0 & 0 \\ 0 & -\mu/r^3 & 0 & 0 & 0 & 0 \\ 0 & 0 & -\mu/r^3 & 0 & 0 & 0 \end{bmatrix}}_{B} \begin{bmatrix} x \\ y \\ z \\ V_x \\ V_y \\ V_z \end{bmatrix} \tag{3.62}$$

Additionally, to get the state transition matrix for the observation time t_i, the equations of variation can be numerically integrated as

$$\frac{d}{dt}\,\Phi(t,t_0) \;=\; A(t)\Phi(t,t_0) \tag{3.63}$$

where $A = \nabla f$

$$A(t) = \begin{bmatrix} \frac{\partial f_1}{\partial x} & \frac{\partial f_1}{\partial y} & \frac{\partial f_1}{\partial z} & \frac{\partial f_1}{\partial V_x} & \frac{\partial f_1}{\partial V_y} & \frac{\partial f_1}{\partial V_z} \\ \frac{\partial f_2}{\partial x} & \frac{\partial f_2}{\partial y} & \frac{\partial f_2}{\partial z} & \frac{\partial f_2}{\partial V_x} & \frac{\partial f_2}{\partial V_y} & \frac{\partial f_2}{\partial V_z} \\ \frac{\partial f_3}{\partial x} & \frac{\partial f_3}{\partial y} & \frac{\partial f_3}{\partial z} & \frac{\partial f_3}{\partial V_x} & \frac{\partial f_3}{\partial V_y} & \frac{\partial f_3}{\partial V_z} \\ \frac{\partial f_4}{\partial x} & \frac{\partial f_4}{\partial y} & \frac{\partial f_4}{\partial z} & \frac{\partial f_4}{\partial V_x} & \frac{\partial f_4}{\partial V_y} & \frac{\partial f_4}{\partial V_z} \\ \frac{\partial f_5}{\partial x} & \frac{\partial f_5}{\partial y} & \frac{\partial f5}{\partial z} & \frac{\partial f_5}{\partial V_x} & \frac{\partial f_5}{\partial V_y} & \frac{\partial f_5}{\partial V_z} \\ \frac{\partial f_6}{\partial x} & \frac{\partial f_6}{\partial y} & \frac{\partial f_6}{\partial z} & \frac{\partial f_6}{\partial V_x} & \frac{\partial f_6}{\partial V_y} & \frac{\partial f_6}{\partial V_z} \end{bmatrix} \tag{3.64}$$

Substituting the the equations we get

$$A = \begin{bmatrix} \frac{\partial V_x}{\partial x} & \frac{\partial V_x}{\partial y} & \frac{\partial V_x}{\partial z} & \frac{\partial V_x}{\partial V_x} & \frac{\partial V_x}{\partial V_y} & \frac{\partial V_x}{\partial V_z} \\ \frac{\partial V_y}{\partial x} & \frac{\partial V_y}{\partial y} & \frac{\partial V_y}{\partial z} & \frac{\partial V_y}{\partial V_x} & \frac{\partial V_y}{\partial V_y} & \frac{\partial V_y}{\partial V_z} \\ \frac{\partial V_z}{\partial x} & \frac{\partial V_z}{\partial y} & \frac{\partial V_z}{\partial z} & \frac{\partial V_z}{\partial V_x} & \frac{\partial V_z}{\partial V_y} & \frac{\partial V_z}{\partial V_z} \\ \frac{\partial(-\frac{\mu x}{r^3})}{\partial x} & \frac{\partial(-\frac{\mu x}{r^3})}{\partial y} & \frac{\partial(-\frac{\mu x}{r^3})}{\partial z} & \frac{\partial(-\frac{\mu x}{r^3})}{\partial V_x} & \frac{\partial(-\frac{\mu x}{r^3})}{\partial V_y} & \frac{\partial(-\frac{\mu x}{r^3})}{\partial V_z} \\ \frac{\partial(-\frac{\mu y}{r^3})}{\partial x} & \frac{\partial(-\frac{\mu y}{r^3})}{\partial y} & \frac{\partial f5}{\partial z} & \frac{\partial(-\frac{\mu y}{r^3})}{\partial V_x} & \frac{\partial(-\frac{\mu y}{r^3})}{\partial V_y} & \frac{\partial(-\frac{\mu y}{r^3})}{\partial V_z} \\ \frac{\partial(-\frac{\mu z}{r^3})}{\partial x} & \frac{\partial(-\frac{\mu z}{r^3})}{\partial y} & \frac{\partial(-\frac{\mu z}{r^3})}{\partial z} & \frac{\partial(-\frac{\mu z}{r^3})}{\partial V_x} & \frac{\partial(-\frac{\mu z}{r^3})}{\partial V_y} & \frac{\partial(-\frac{\mu z}{r^3})}{\partial V_z} \end{bmatrix} \tag{3.65}$$

and when we get the partial derivatives, we have

$$A = \begin{bmatrix} \phi & I \\ A_{rr} & \phi \end{bmatrix} \tag{3.66}$$

where I is the identity matrix and ϕ represents the null matrix. As in Wiesel's algorithm A_{rr} can be created as

$$A_{rr} = \begin{bmatrix} -\frac{\mu}{r^3} + \frac{3\mu x^2}{r^5} & \frac{3\mu xy}{r^5} & \frac{3\mu xz}{r^5} \\ \frac{3\mu xy}{r^5} & -\frac{\mu}{r^3} + \frac{3\mu y^2}{r^5} & \frac{3\mu yz}{r^5} \\ \frac{3\mu xz}{r^5} & \frac{3\mu yz}{r^5} & -\frac{\mu}{r^3} + \frac{3\mu z^2}{r^5} \end{bmatrix} \tag{3.67}$$

Now, if we write the equations of variation in matrix form we get

$$\begin{bmatrix} \dot{\Phi}_{11} & \dot{\Phi}_{12} & \cdots & \dot{\Phi}_{16} \\ \dot{\Phi}_{21} & \dot{\Phi}_{22} & \cdots & \dot{\Phi}_{26} \\ \vdots & \vdots & \ddots & \vdots \\ \dot{\Phi}_{61} & \dot{\Phi}_{62} & \cdots & \dot{\Phi}_{66} \end{bmatrix} = \begin{bmatrix} A_{11} & A_{12} & \cdots & A_{16} \\ A_{21} & A_{22} & \cdots & A_{26} \\ \vdots & \vdots & \ddots & \vdots \\ A_{61} & A_{62} & \cdots & A_{66} \end{bmatrix} \begin{bmatrix} \Phi_{11} & \Phi_{12} & \cdots & \Phi_{16} \\ \Phi_{21} & \Phi_{22} & \cdots & \Phi_{26} \\ \vdots & \vdots & \ddots & \vdots \\ \Phi_{61} & \Phi_{62} & \cdots & \Phi_{66} \end{bmatrix} \tag{3.68}$$

In order to numerically integrate Equation (3.68) using $MATLAB$ it has to be modified. Also, the state vector and the state transition matrix should be integrated simultaneously. Finally, the matrix form that can be integrated is set up as

$$\begin{bmatrix} \dot{\Phi}_1 \\ \dot{\Phi}_2 \\ \vdots \\ \dot{\Phi}_6 \\ \dot{X} \end{bmatrix}_{42\times 1} = \begin{bmatrix} A_{11}I_{6\times 6} & A_{12}I_{6\times 6} & \cdots & A_{16}I_{6\times 6} & 0_{6\times 6} \\ A_{21}I_{6\times 6} & A_{22}I_{6\times 6} & \cdots & A_{26}I_{6\times 6} & 0_{6\times 6} \\ \vdots & \vdots & \ddots & \vdots & \vdots \\ A_{61}I_{6\times 6} & A_{62}I_{6\times 6} & \cdots & A_{66}I_{6\times 6} & 0_{6\times 6} \\ 0_{6\times 6} & 0_{6\times 6} & \cdots & 0_{6\times 6} & B \end{bmatrix}_{42\times 42} \begin{bmatrix} \Phi_1 \\ \Phi_2 \\ \vdots \\ \Phi_6 \\ X \end{bmatrix}_{42\times 1} \tag{3.69}$$

where

$$\Phi_1 = \begin{bmatrix} \Phi_{11} \\ \Phi_{12} \\ \Phi_{13} \\ \Phi_{14} \\ \Phi_{15} \\ \Phi_{16} \end{bmatrix}, \Phi_2 = \begin{bmatrix} \Phi_{21} \\ \Phi_{22} \\ \Phi_{23} \\ \Phi_{24} \\ \Phi_{25} \\ \Phi_{26} \end{bmatrix}, \Phi_3 = \begin{bmatrix} \Phi_{31} \\ \Phi_{32} \\ \Phi_{33} \\ \Phi_{34} \\ \Phi_{35} \\ \Phi_{36} \end{bmatrix}, ...\Phi_6 = \begin{bmatrix} \Phi_{61} \\ \Phi_{62} \\ \Phi_{63} \\ \Phi_{64} \\ \Phi_{65} \\ \Phi_{66} \end{bmatrix} \tag{3.70}$$

$$\dot{\Phi}_1 = \begin{bmatrix} \dot{\Phi}_{11} \\ \dot{\Phi}_{12} \\ \dot{\Phi}_{13} \\ \dot{\Phi}_{14} \\ \dot{\Phi}_{15} \\ \dot{\Phi}_{16} \end{bmatrix}, \dot{\Phi}_2 = \begin{bmatrix} \dot{\Phi}_{21} \\ \dot{\Phi}_{22} \\ \dot{\Phi}_{23} \\ \dot{\Phi}_{24} \\ \dot{\Phi}_{25} \\ \dot{\Phi}_{26} \end{bmatrix}, \dot{\Phi}_3 = \begin{bmatrix} \dot{\Phi}_{31} \\ \dot{\Phi}_{32} \\ \dot{\Phi}_{33} \\ \dot{\Phi}_{34} \\ \dot{\Phi}_{35} \\ \dot{\Phi}_{36} \end{bmatrix}, ...\dot{\Phi}_6 = \begin{bmatrix} \dot{\Phi}_{61} \\ \dot{\Phi}_{62} \\ \dot{\Phi}_{63} \\ \dot{\Phi}_{64} \\ \dot{\Phi}_{65} \\ \dot{\Phi}_{66} \end{bmatrix} \tag{3.71}$$

The time interval of the numerical integration can be any time period throughout the flight time of the ASAT missile with selectable time steps. The initial conditions should be $I_{6\times6}$ for the state transition matrix Φ and any selected state on the reference trajectory for the initial state of the ASAT missile. Returning to Wiesel's algorithm, the filter calculates residuals as $r_i = z_i - G(X)$. H_i and the

observation matrix $T_i = Hi\Phi$ are calculated for each time step of the observations. The covariance of the correction $P_{\delta X}$ and the correction vector $\delta X(t_0)$ at epoch time are calculated by the filter using running sums at each iteration.

$$P_{\delta X} = \left(\sum_i T_i^T Q_i^{-1} T_i \right)^{-1} \tag{3.72}$$

$$\delta X(t_0) = P_{\delta X} \sum_i T_i^T Q_i^{-1} r_i \tag{3.73}$$

Given in Equation 3.72 and Equation 3.73, $\left(\sum_i T_i^T Q_i^{-1} T_i \right)^{-1}$ should be invertible to find δX.Finally, the filter corrects the reference trajectory state at epoch time.

$$X_{ref+1}(t_0) = X_{ref}(t_0) + \delta X(t_0) \tag{3.74}$$

After finding the corrected state at epoch time the filter uses this new state as the initial condition of the ASAT trajectory. The filter repeats the iteration until it reaches the convergence criteria. The convergence criteria can come from the covariance matrix. It is determined that if the correction to each element of the state vector is smaller than half of the square root of the corresponding diagonal element of the covariance matrix there is no need to continue iterating. To explain convergence criteria symbolically, for the components of the last computed state vector if all of the following are simultaneously true

$$
\begin{aligned}
\delta x &< 0.5\sqrt{P_{\delta X}(1,1)} \\
\delta y &< 0.5\sqrt{P_{\delta X}(2,2)} \\
\delta z &< 0.5\sqrt{P_{\delta X}(3,3)} \\
\delta V_x &< 0.5\sqrt{P_{\delta X}(4,4)} \\
\delta V_y &< 0.5\sqrt{P_{\delta X}(5,5)} \\
\delta V_z &< 0.5\sqrt{P_{\delta X}(6,6)}
\end{aligned}
$$

then the filter stops iterating, takes the last computed state at epoch time t_0 as initial conditions, propagates the state in time and finds the position and velocity of the ASAT missile at the time of impact. The process of the filter is shown in Figures 3.5, 3.6, and 3.7.

3.5 Frames

Describing an orbit is only possible with a suitable inertial reference frame. Coordinate frames, as well defined and detailed in many documents, differ from each other depending on their definition of the origin, the fundamental plane and the principal axis. Only two of these coordinate frames, the ones that are used in this document, will be described in this section.

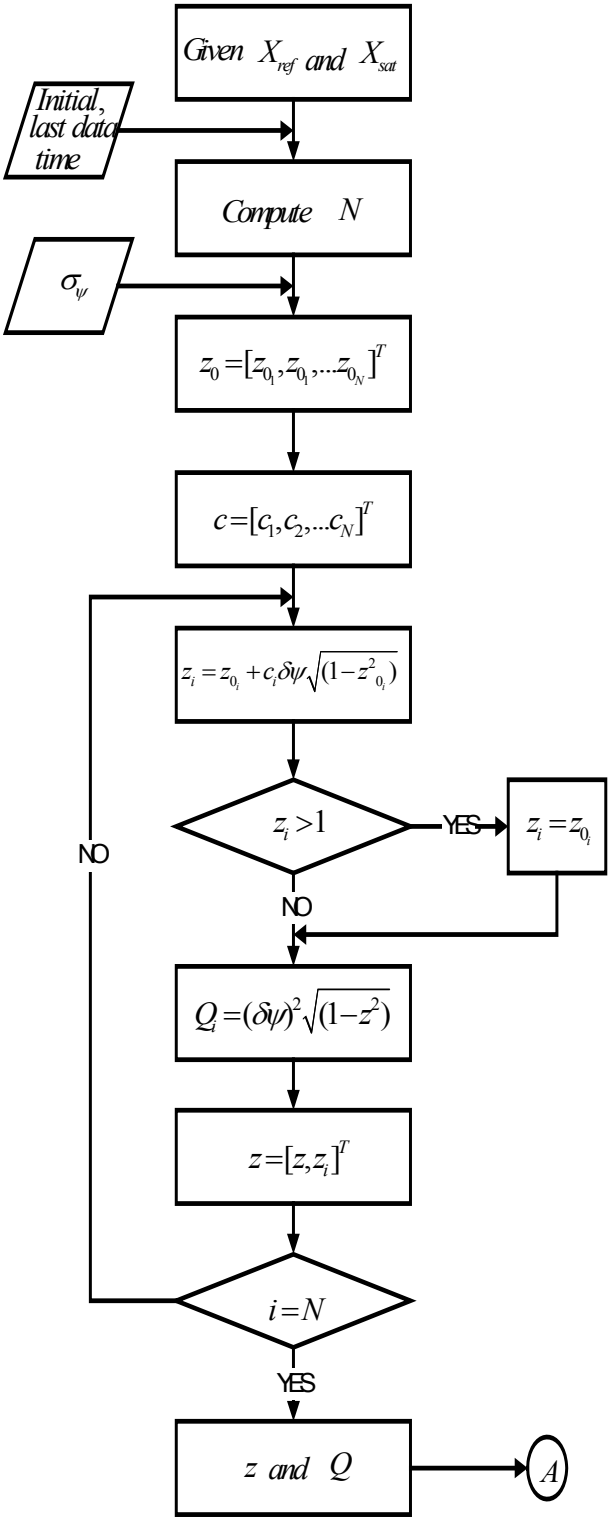

Figure 3.5: Algorithm for Least Squares Estimation Filter (Part 1 of 3).

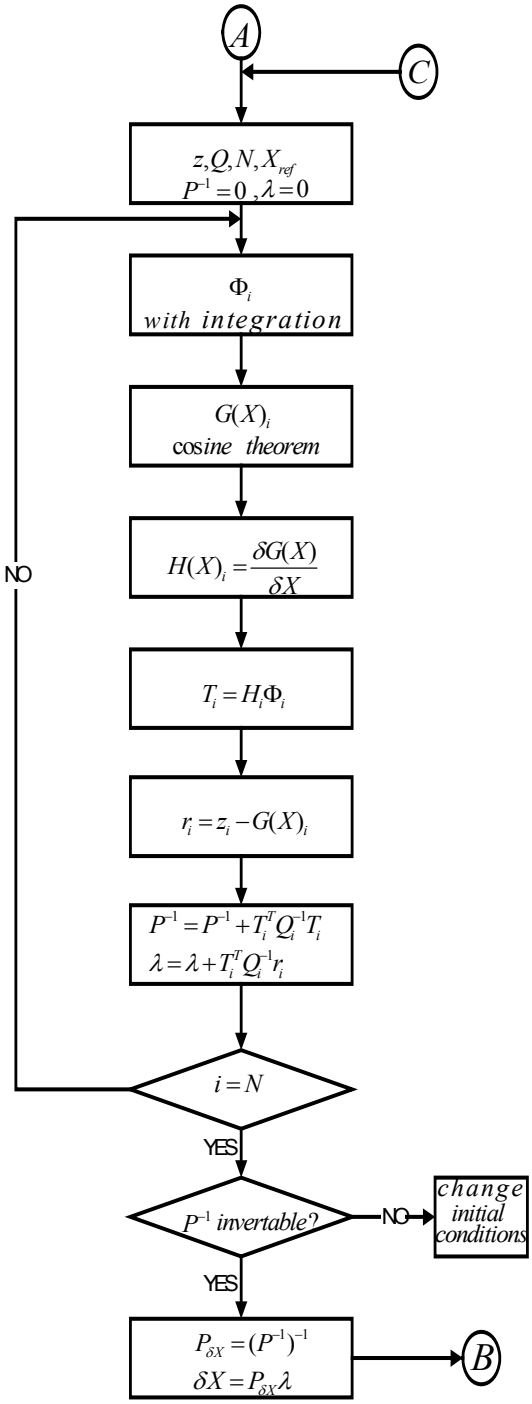

Figure 3.6: Algorithm for Least Squares Estimation Filter (Part 2 of 3).

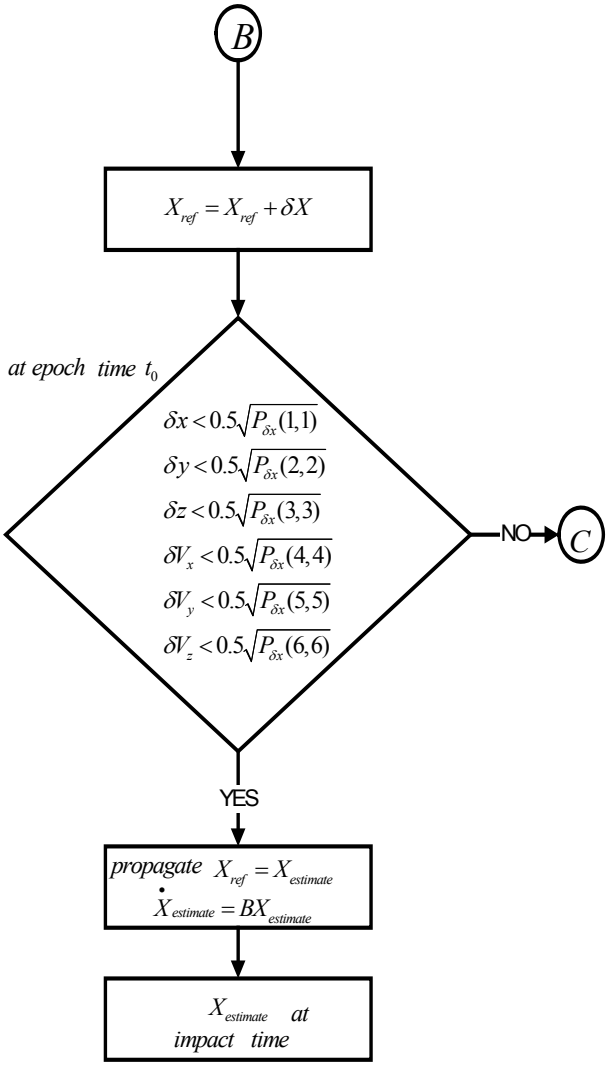

Figure 3.7: Algorithm for Least Squares Estimation Filter (Part 3 of 3).

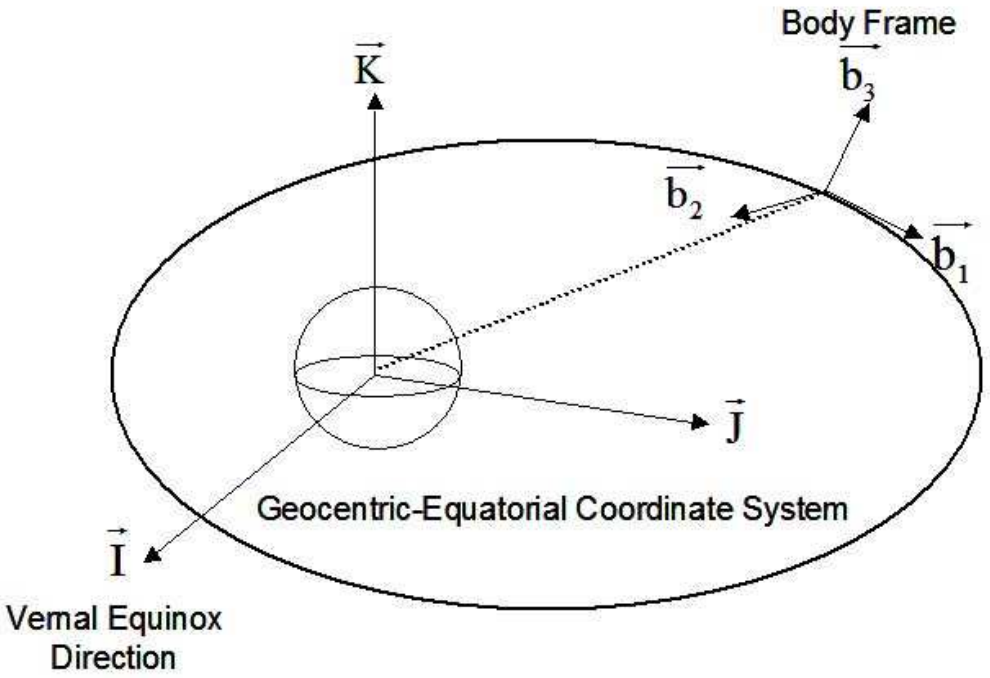

Figure 3.8: Geocentric-Equatorial Coordinate Frame and Satellite Body Frame.

While describing the motion of the objects orbiting the earth, using the geocentric-equatorial coordinate frame is more convenient than other coordinate systems. As depicted in Figure 3.8, the origin of the geocentric-equatorial coordinate frame is the center of the earth and its fundamental plane is the same with the earth's equatorial plane. The positive $\vec{I}$ axis, which is the principle axis, points to the vernal equinox direction. The $\vec{K}$ axis is perpendicular to the fundamental plane and points in the direction of the North Pole. The $\vec{J}$ axis completes the right handed set of coordinate axes. Finally, it is important to emphasize that the geocentric-equatorial coordinate frame is not rotating with the earth and except for the precession of the equinoxes the coordinate system is relatively fixed with respect to the stars.

The body frame of the satellite is used to calculate and demonstrate the position of the ASAT missile with respect to the satellite at the time of impact. The origin of the body frame is the center of gravity of the satellite. The fundamental plane of this coordinate system is the orbital plate of the satellite. The positive principal axis $\vec{b_1}$ is pointing in the direction of the velocity vector of the satellite. The $\vec{b_3}$ axis is always perpendicular to the orbital plane. The $\vec{b_2}$ axis points roughly to the earth as the third element of the coordinate system, composed of three perpendicular unit vectors. As its name implies, the body frame is fixed with respect to the satellite, especially when the two-body dynamics assumes that the satellite's total mass is concentrated at its center of gravity. Although it is non-rotating when compared to the satellite, the body frame rotates with respect to the inertial frame, stars and the earth. The rotation matrix that converts a vector from the initial frame to the body frame can be created as

$$\begin{aligned} R^{bi} &= \left\{\hat{b}\right\}\{\hat{i}\}^T \\ R^{bi} &= \begin{bmatrix} \vec{b_1}\cdot\vec{i_1} & \vec{b_1}\cdot\vec{i_2} & \vec{b_1}\cdot\vec{i_3} \\ \vec{b_2}\cdot\vec{i_1} & \vec{b_2}\cdot\vec{i_2} & \vec{b_2}\cdot\vec{i_3} \\ \vec{b_3}\cdot\vec{i_1} & \vec{b_3}\cdot\vec{i_2} & \vec{b_3}\cdot\vec{i_3} \end{bmatrix} \end{aligned} \tag{3.75}$$

where $\hat{b} = [\vec{b_1}, \vec{b_2}, \vec{b_3}]^T$ and $\hat{i} = [\vec{i_1}, \vec{i_2}, \vec{i_3}]^T$. The vectors $\vec{i_1}, \vec{i_2}$ and $\vec{i_3}$ are the unit vectors in the directions of $\vec{I}, \vec{J}, \vec{K}$ respectively.

Since we have the state vector of the targeted satellite in the inertial frame, the principle axis of the selected body frame $\left[\vec{b_1}\right]_i$ with respect to inertial frame can be found by normalizing the satellite's velocity vector.

$$\left[\vec{b_1}\right]_i = \frac{[V_x, V_y, V_z]_{sat}}{\sqrt{(V_x)^2 + (V_y)^2 + (V_z)^2}} \tag{3.76}$$

Then, taking the cross product of $\left[\vec{b_1}\right]_i$ with the position vector of the satellite and normalizing that vector, we get $\left[\vec{b_3}\right]_i$, pointing in the direction of angular momentum vector,

$$\left[\vec{b_3}\right]_i = \frac{\left[\vec{b_1}\right]_i \times [x, y, z]_i}{|\left[\vec{b_1}\right]_i \times [x, y, z]_i|} \tag{3.77}$$

and in order to calculate $\left[\vec{b_2}\right]_i$, cross product should be used again

$$\left[\vec{b_2}\right]_i = \frac{\left[\vec{b_1}\right]_i \times \left[\vec{b_3}\right]_i}{|\left[\vec{b_1}\right]_i \times \left[\vec{b_3}\right]_i|} \tag{3.78}$$

Given $\left[\vec{b}\right]_i$ the rotation matrix from inertial to body frame can be achieved easily in two steps as

$$R^{ib} = \begin{bmatrix} \left[\vec{b_1}\right]_i^T & \left[\vec{b_2}\right]_i^T & \left[\vec{b_3}\right]_i^T \end{bmatrix} \tag{3.79}$$

$$R^{bi} = R_{ib}^{T} \tag{3.80}$$

The rotation matrix R^{bi} was used to express the position of the ASAT on its estimated trajectory at the time of closest pass.

$$\begin{bmatrix} x \\ y \\ z \end{bmatrix}_b = R^{bi} \begin{bmatrix} x \\ y \\ z \end{bmatrix}_i \tag{3.81}$$

This miss distance changes with the inputs of the filter. The results will be detailed in Chapter IV.

IV. The Results and the Analysis

4.1 Chapter overview

In this chapter, the sensitivity of the filter was analyzed by comparing estimated miss distances of the ASAT missile with respect to the targeted satellite. As previously described, the inputs of the filter that change the estimations were the sensor accuracy and the frequency of the observations. The filter was designed such that the accuracy of the sensor could be entered in arcseconds and the number of observations were entered as the measurement amount per second. For each set of these two inputs the filter generated an estimated state vector at epoch time and this state vector was propagated in time to find the estimated state of the ASAT at the predetermined impact time. This state vector was defined and calculated with respect to the inertial frame. Finally this vector was rotated and defined with respect to the body frame of the satellite. The rotation of the state vector was described in the previous chapter. Only the $\left[\vec{b_2}\right]$ and the $\left[\vec{b_3}\right]$ components of the state vector were considered as the cross track and the radial components of the miss distance respectively. For the analysis of the results the Monte Carlo simulation was used. The flow diagram of this analysis is shown in Figure 4.1.

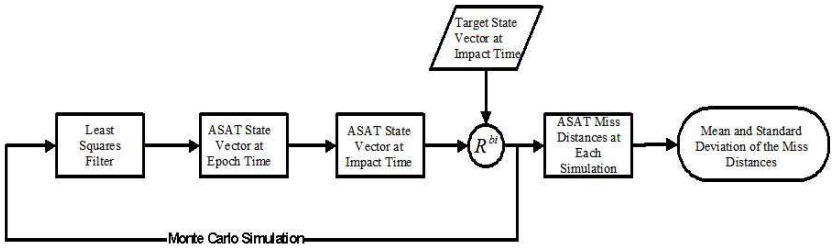

Figure 4.1: Flow Diagram of the Monte Carlo simulations.

4.2 Monte Carlo Simulations

Monte Carlo simulations take the slightly different initial inputs for a system and iterates them in order to find different results based on the accuracy of the iteration process and dynamics. After getting enough different results some analysis like mean and standard deviation of the results can be done. The Monte Carlo simulations are advantageous because they are easy to be performed and only the system dynamics are needed. [20]

In this research, Monte Carlo simulations were used to generate different estimated state vectors of the ASAT missile with respect to the target satellite at the impact time. At each run of the Monte Carlo simulation, the closest cross track and radial miss distances of the estimated ASAT position were calculated. The mean value of the miss distances at the plane perpendicular to the satellite's velocity vector was calculated as

$$x_{mean} = \sum_{i=1}^{N} \frac{x_i}{N} \tag{4.1}$$

and standard deviation of the miss distances was calculated as

$$\sigma_x = \sqrt{\sum_{i=1}^{N} \frac{(x_i - x_{mean})^2}{N}} \tag{4.2}$$

where N represents the amount of Monte Carlo runs. In figures of the results, an ellipsoid, which had an origin at the mean of the miss distances, is shown. The semi-major and the semi-minor axis of the ellipsoid represents the standard deviation at

the associated axis direction. Also the observation interval and the sensor accuracy is labeled in each figure. When the input sets were changed as more measurement data per second or as more precise sensor accuracy the miss distances became smaller. These different input sets were given to the filter and after Monte Carlo simulations the outputs were calculated and shown in figures.

4.3 Comparison of Filter Estimates

Different sets of inputs were created in an observation amount range between 1 observation per second to 1000 observations per second and a sensor accuracy range between $1 Arcsecod$ and $1/1000 Arcsecod$. When inputs of less than 1 observations per second was considered the least squares filter was not able to compute an estimate because the observability condition (*the matrix* $T^T Q^{-1} T$ *must be invertable*) defined by Wiesel could not be met. The sensor accuracies more precise than 1/1000 *Arcsecond* were not considered. Sensors with an accuracy of 1 *Arcsecond* were being used at present time, so anything better than 1/1000 *Arcsecond* was considered beyond near-term capabilities.

Initially, the improvement of the filter estimates with the sensor accuracy based on certain amount of observations was described. Then, the comparison of the estimation's improvement due to different observation amounts were shown in this section. For the following different cases it was seen that although the filter had a bias, the more accurate sensor or the higher observation rates results in better performance of the filter.

4.3.1 1 *Observation per Second.* For the case in which the the filter inputs were composed of 1 observation per second, it was seen that the sensor accuracy should be at least 0.01 *Arcsecod*. In this case the position estimates of the ASAT missile with respect to the satellite were shown in Figure 4.2.

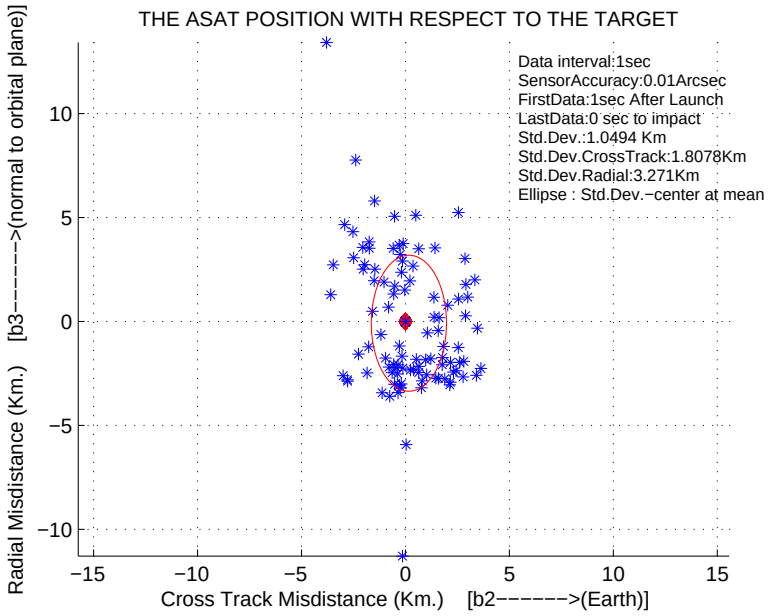

Figure 4.2: Estimated position of ASAT at Impact Time (Data interval: 1*sec*; Accuracy:0.01 *Arcsecod*).

When the sensor accuracy is increased to 0.001 *Arcseconds* the miss distances becomes smaller as shown in Figure 4.3. For these two cases 100 Monte Carlo runs established and the improvement of the filter estimations parallel to the sensor accuracy was observed. In reality the satellite would need to stop taking observations and make a maneuver to defeat the missile at some time before the impact, so the estimate without this last observations should be calculated. Also, to make the scenario a little bit more realistic it could be assumed that the sensor could not take measurements for some time after the launch of the missile. Given these facts the filter

was tried to generate estimates with a set of data ignoring some observations from the beginning and the last part of the missile's trajectory. Again the observability condition limited the filter and it was seen that the filter should have almost all of the observations in 1 observation per second case.

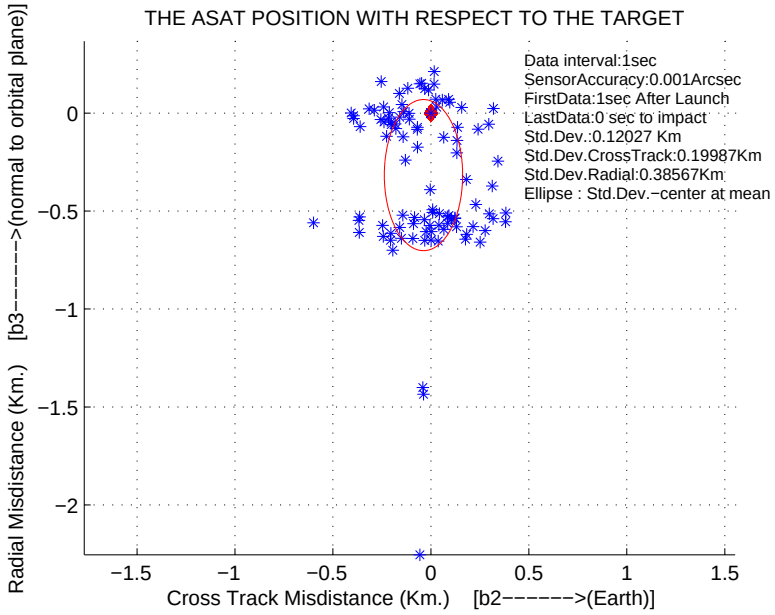

Figure 4.3: Estimated position of ASAT at Impact Time (Data interval: 1*sec*; Accuracy:0.001 *Arcsecod*).

The standard deviations of ASAT positions, estimated at impact time based on one data per second are shown in Table 4.1.

Table 4.1: Standard Deviations of ASAT Miss Distances for *1* Observation per Second.

Accuracy	**Standard Deviations** (km)		
(Arcsecond)	**Total**	**Cross Track**	**Radial**
0.01	1.0494	1.8078	3.271
0.001	0.1203	0.19987	0.39567

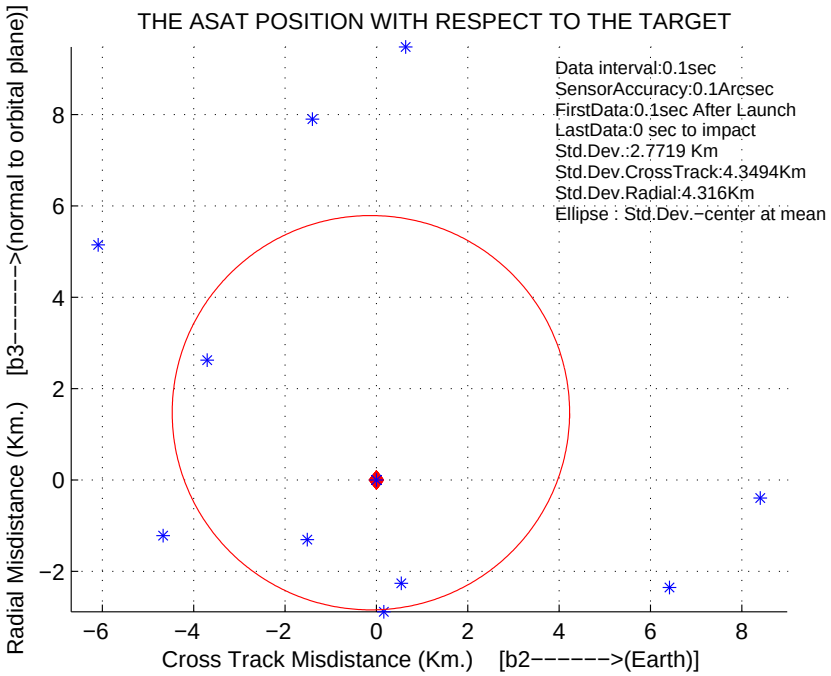

Figure 4.4: Estimated position of ASAT at Impact Time (Data interval: 0.1*sec*; Accuracy:0.1 *Arcsecod*).

4.3.2 10 *Observations per Second.* When the observation amount was increased it was discovered that the filter could generate an estimate with a senor accuracy of 0.1 *Arcsecond*. The estimated positions of the ASAT calculated with 10 observations per second and different sensor accuracies are shown in Figures 4.4, 4.5 and 4.6.

It is clear in the figures that the estimations of the filter gets closer to the reference trajectory and as a result the ASAT missile's miss distance at the impact time gets smaller and smaller when the sensor becomes more accurate. The improvement of the estimates can be seen together in Table 4.2.

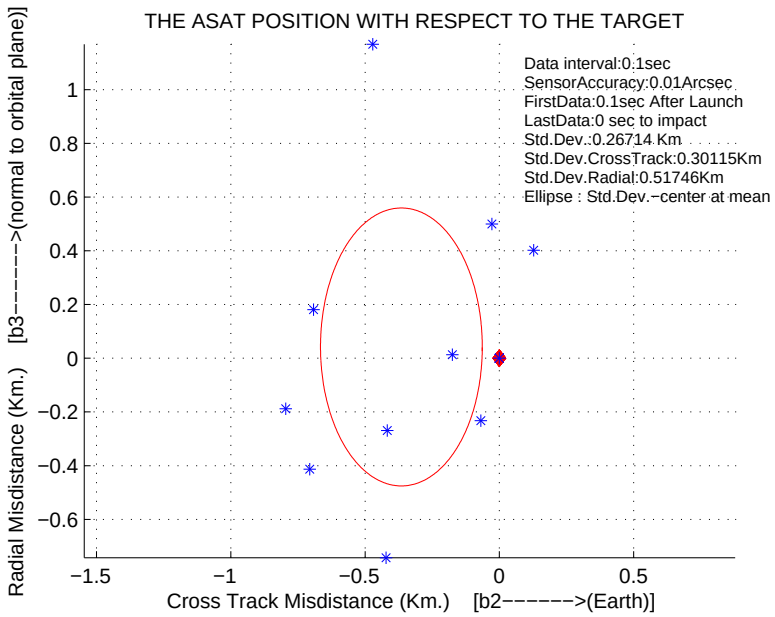

Figure 4.5: Estimated position of ASAT at Impact Time (Data interval: 0.1*sec*; Accuracy:0.01 *Arcsecod*).

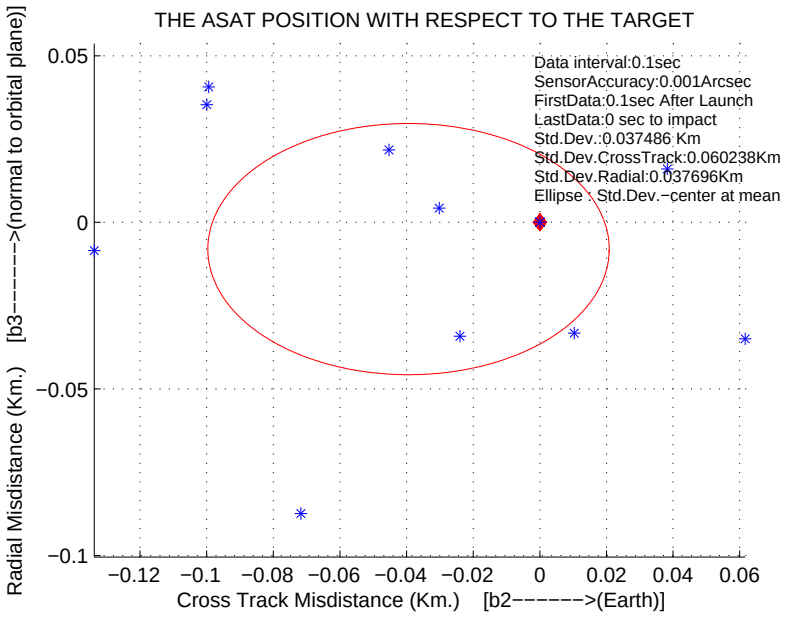

Figure 4.6: Estimated position of ASAT at Impact Time (Data interval: 0.1*sec*; Accuracy:0.001 *Arcsecod*).

Table 4.2: Standard Deviations of ASAT Miss Distances for *10* Observations per Second.

Accuracy	**Standard Deviations** (km)		
(Arcsecond)	**Total**	**Cross Track**	**Radial**
0.1	2.7719	4.3494	4.316
0.01	0.26714	0.30115	0.51746
0.001	0.03749	0.060238	0.037696

4.3.3 100 *Observations per Second.* When the sensor begun to perform a hundred obsevations in one second not only the whole trajectory observation case but also reduced data estimation case started to establish better results. The filter could generate better estimations when data was cut from the beginning and the end of the ASAT missile's trajectory. The results when the sensor could get observations throughout the entire flight time of the missile were shown in Figures 4.7, 4.8, 4.9 and the standard deviations of the results for different sensor accuracies were shown in Table 4.3.

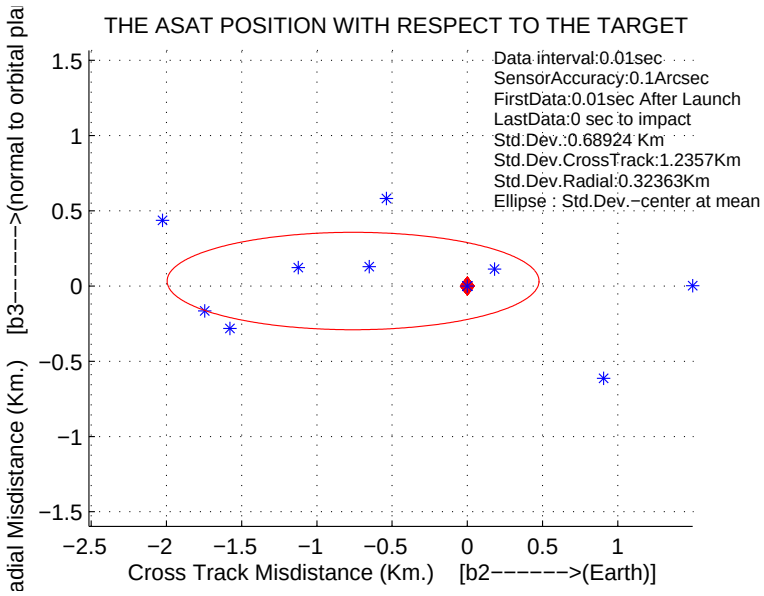

Figure 4.7: Estimated position of ASAT at Impact Time (Data interval: 0.01*sec*; Accuracy:0.1 *Arcsecod*).

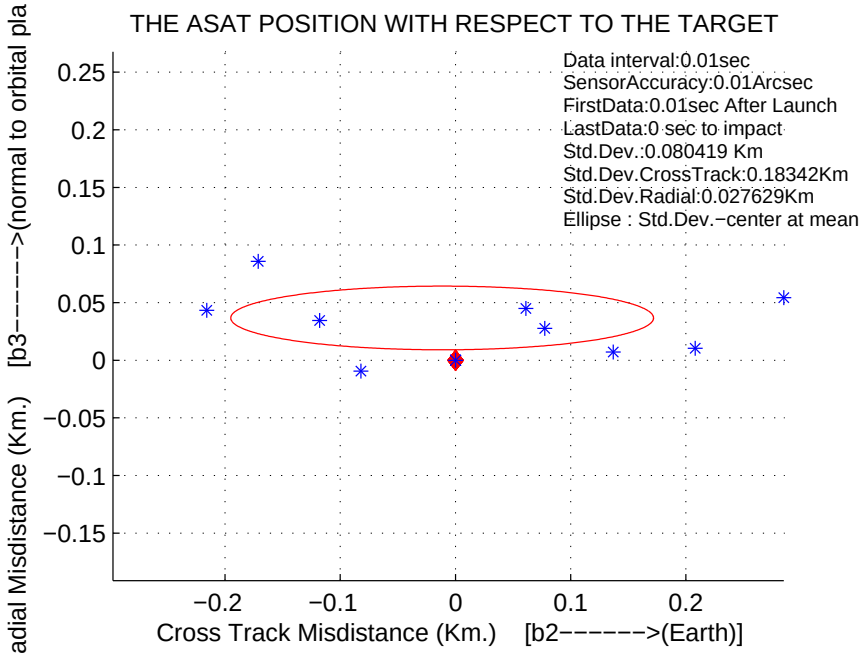

Figure 4.8: Estimated position of ASAT at Impact Time (Data interval: 0.01*sec*; Accuracy:0.01 *Arcsecod*).

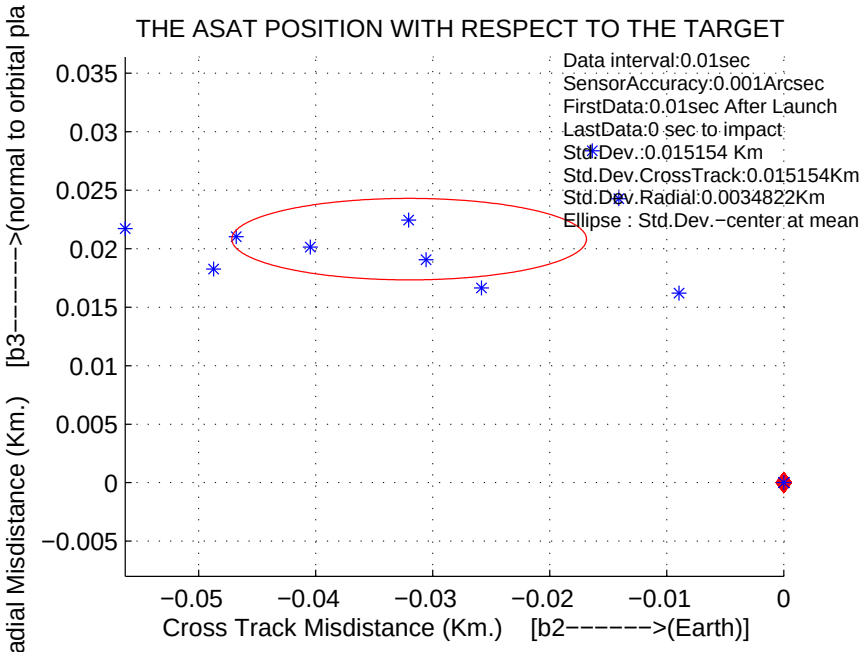

Figure 4.9: Estimated position of ASAT at Impact Time (Data interval: 0.01*sec*; Accuracy:0.001 *Arcsecod*).

Table 4.3: Standard Deviations of ASAT Miss Distances for *100* Observations per Second.

Accuracy	**Standard Deviations** (km)		
(Arcsecond)	**Total**	**Cross Track**	**Radial**
0.1	0.68924	1.2357	0.32363
0.01	0.080419	0.18342	0.027629
0.001	0.015154	0.015154	0.003482

4.3.4 1000 *Observations per Second.* When the case in which the sensor performs 1000 observations per second was considered the total amount of measurements for this particular scenario reached up to $500,000$. Since the length of the matrixes was too large the numerical integration became difficult to handle with ordinary home-use computers with limited processors and memory. The problem was still solvable but took a lot of time (i.e. approximately two days) to get the results of the filter's one or two estimates. Because of the limited time of this research only two or three filter estimates based on input sets of 1000 observations per second and different sensor accuracies were generated. The results were shown in Figures 4.10, 4.11, 4.12. Even though only two or three computations could be established the results were shown in the figures and the standard deviations for each axis had been computed and summarized in Table 4.4 in order to compare with the other cases. The standard deviations could not be accurate enough due to the limited runs of the Monte Carlo simulation. However, the order of the miss distances of ASAT missile at impact time can give a sense and make the comparisons more meaningful. The mean values of the miss distances are shown in Table 4.5.

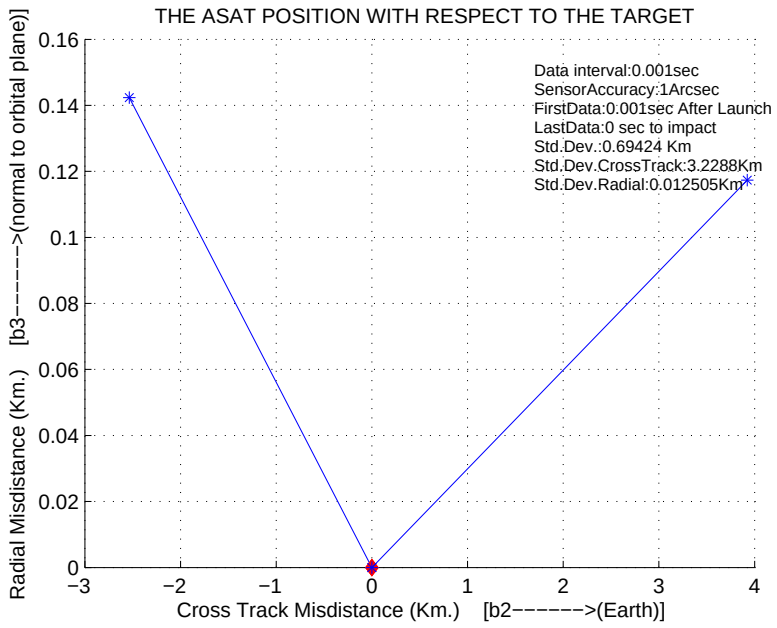

Figure 4.10: Estimated position of ASAT at Impact Time (Data interval: 0.001*sec*; Accuracy:1 *Arcsecod*).

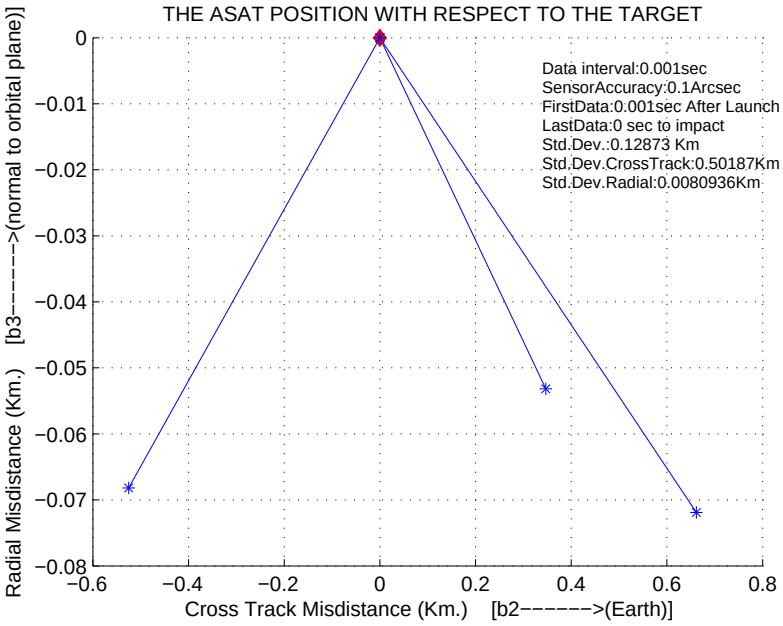

Figure 4.11: Estimated position of ASAT at Impact Time (Data interval: 0.001*sec*; Accuracy:0.1 *Arcsecod*).

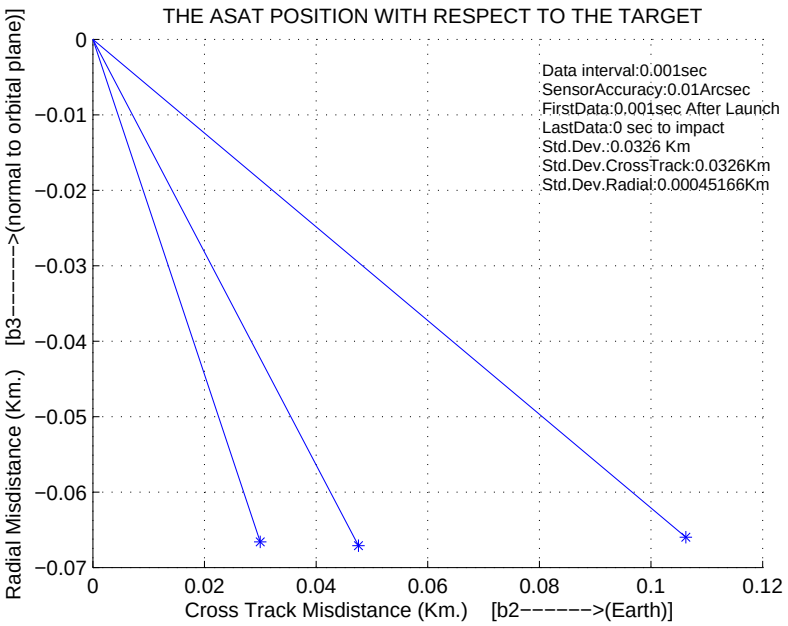

Figure 4.12: Estimated position of ASAT at Impact Time (Data interval: 0.001*sec*; Accuracy:0.01 *Arcsecod*).

Table 4.4: Standard Deviations of ASAT Miss Distances for *1000* Observations per Second.

Accuracy	**Standard Deviations** (km)		
(Arcsecond)	**Total**	**Cross Track**	**Radial**
1	0.69424	3.2288	0.012505
0.1	0.12873	0.50187	0.00809
0.01	0.0326	0.0326	0.00045

Table 4.5: Mean Values of ASAT Miss Distances for *1000* Observations per Second.

Accuracy	**Mean Values** (km)		
(Arcsecond)	**Total**	**Cross Track**	**Radial**
1	3.23	0.69	0.13
0.1	0.51	0.16	0.064
0.01	0.061	0.0612	0.066

4.3.5 The Filter Estimates in More Realistic Simulations . As mentioned previously, the satellite should stop taking measurements at some time before the

predetermined impact time in order to maneuver and defeat the ASAT missile. Also, in a more realistic simulation the satellite would only be able to catch and start tracking the ASAT missile at some time after the launch. The filter was tested for different cases in which the observation started at a time after the launch and the measurements stopped at a time before the impact. In most trials the observability condition could not be met and the filter could not generate an estimated ASAT trajectory. It has been concluded that as an input to the filter, the observation amount should be at least 10 observations per second in order to accomplish an estimate without observing the entire trajectory from the launch to the impact. The different input sets that resulted with an estimate were pictured in the following figures. For the first condition the filter could calculate an estimated trajectory by tracking the missile from 60 seconds after the launch until 10 seconds before the impact time with an observation rate of 100 observations per second.

In this case, if we assume that the satellite could start the maneuver just after it stopped taking the observations, again assuming that it would maneuver in the radial direction where the standard deviation of the estimated miss distances is larger than the cross track direction and with an assumption that it would maneuver just enough to move out of the standard deviation amount of range,

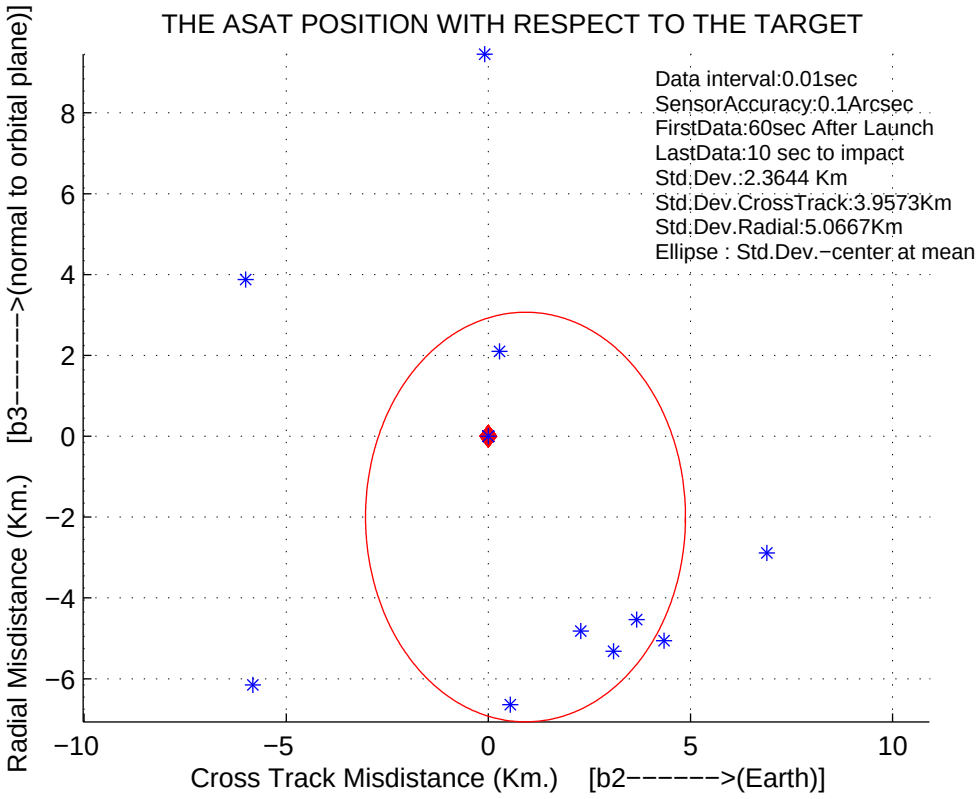

Figure 4.13: (Data interval: $0.01 sec$; Accuracy:0.1 *Arcsecod*;from 60 sec after launch till 10 sec to impact).

$$\begin{aligned} d &= V_0 t + \frac{1}{2} g t^2 \\ 5000m &= \frac{1}{2} g (10)^2 \\ g &\approx 100\ m/sec^2 \end{aligned} \tag{4.3}$$

the acceleration on the satellite will be approximately 100 m/sec^2. In order to generate this acceleration the thrusters on a satellite, which is in the size of FY-1C, should create the force,

$$
\begin{aligned}
F &= ma \qquad (4.4)\\
&\approx 750\ kg \times 100\ m/sec^2\\
F &\approx 75000\ N
\end{aligned}
$$

Although this calculated thrust seems to be a little bit high, there are available engines that can create it. [21] It can be said that if the accuracy of the sensor would be increased, more precise estimations can be generated by the filter, but since this result is reasonable and applicable, the more accurate cases wasn't calculated.

For the next case if the observation amount was reduced to ten measurements per second then the sensor accuracy should be increased in order to have the filter generate an estimate. The calculated estimates were pictured in Figures 4.14, 4.15, 4.16. Using the same maneuver assumptions made for the previous case and the Equations 4.3 and4.4, if the sensor performed 10 observations per second and started to track the ASAT missile 60*seconds* after the launch; the approximate amount of maneuver accelerations of the satellite and the required forces would be like the calculated results shown in Table 4.6. The required thrusts that for the associated accelerations were calculated based on a 750 kg satellite representing FY-1C.

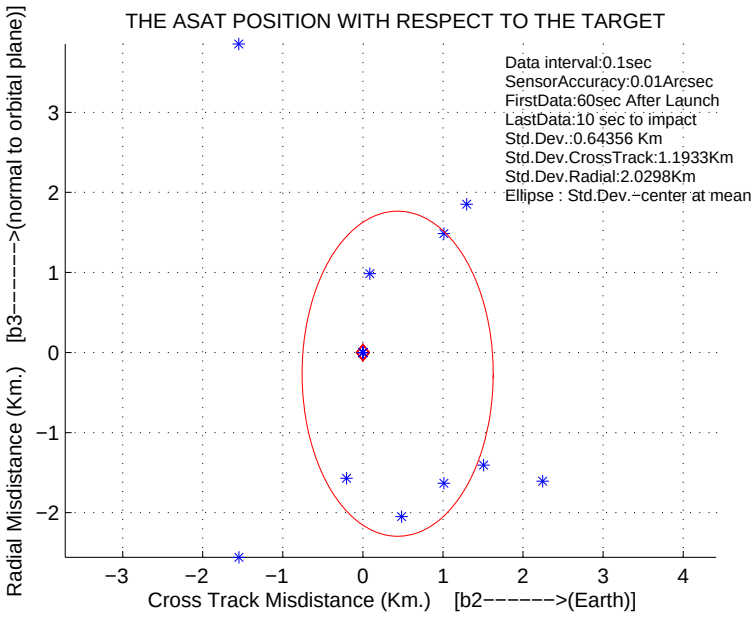

Figure 4.14: (Data interval: 0.1*sec*; Accuracy:0.01 *Arcsecod*;from 60 sec after launch till 10 sec to impact).

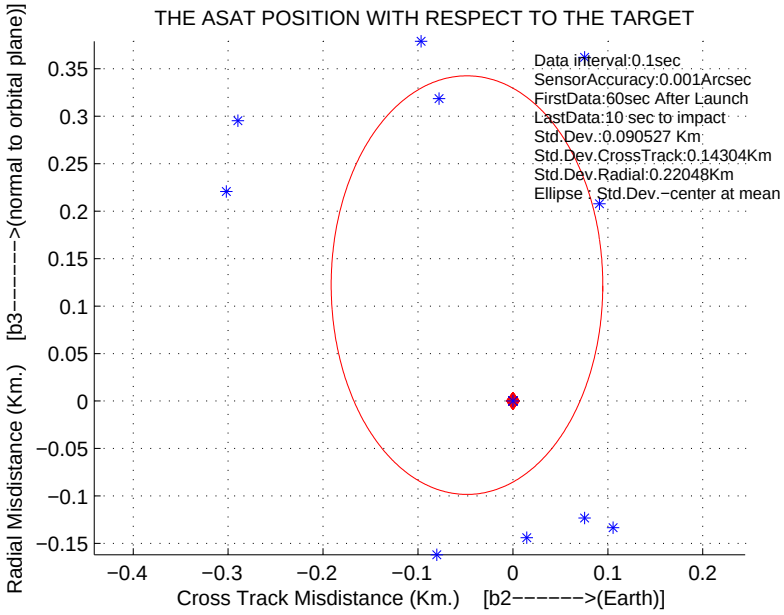

Figure 4.15: (Data interval: 0.1*sec*; Accuracy:0.001 *Arcsecod*;from 60 sec after launch till 10 sec to impact).

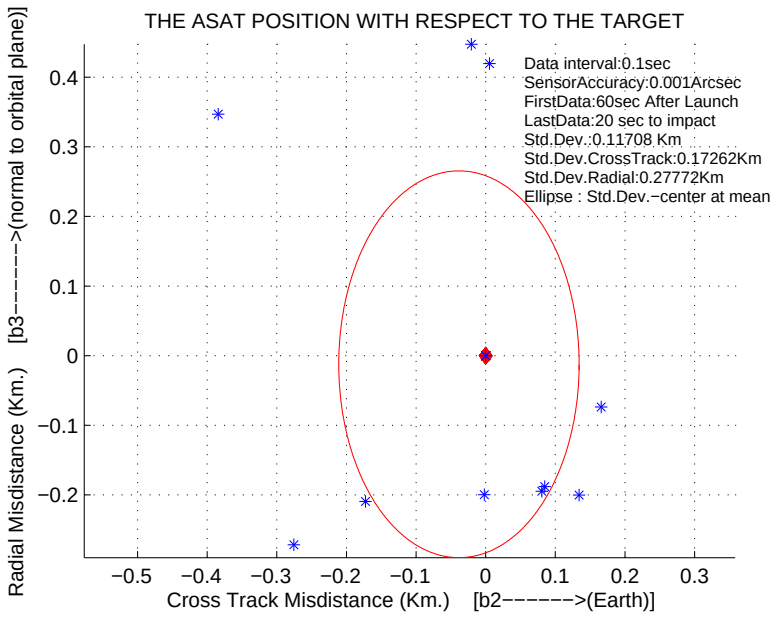

Figure 4.16: (Data interval: $0.1sec$; Accuracy:0.001 *Arcsecod*;from 60 sec after launch till 20 sec to impact).

Table 4.6: Required Accelerations and Forces of Satellite Maneuvers for 10 observations per Second.

Accuracy	**First Data**	**Last Data**	**Aceleration**	**Force**
Arcsecond	sec after Launch	sec before Impact	m/sec^2	N
0.01	60	10	$\approx$ **40**	$\approx$ **30000**
0.001	60	10	$\approx$ **4.4**	$\approx$ **3300**
0.001	60	20	$\approx$ **1.4**	$\approx$ **1050**

4.3.6 Comparison Based on Data Interval or Sensor Accuracy Only. In order to compare the estimates of the least squares filter, the results can be compared while keeping the accuracy constant and changing the observation amount per second. The improvement of the standard deviations can provide an idea about the sensor selection. Since observability condition could not be met at each set of the inputs, only the results of the achievable input sets were shown. For the first condition

when the accuracy was 0.1*Arcsecond* the standard deviation of the miss distances got smaller while the observation amount increased, as seen in Figure 4.17.

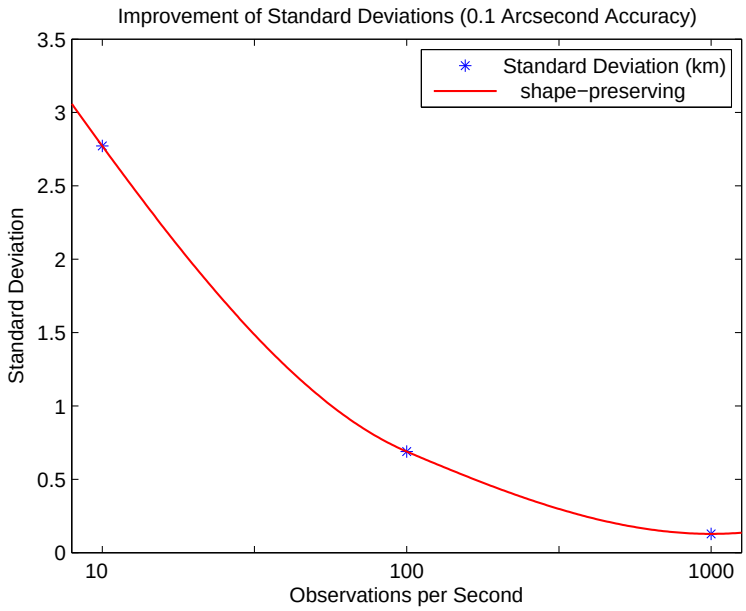

Figure 4.17: Improvement of Standard Deviation (0.1 Arcsecond Accuracy).

When the accuracy was increased to 0.01*Arcsecond* the standard deviation improvement got better as it could be seen in Figure 4.18. Figure 4.19 shows the case in which the accuracy had been improved to 0.001 Arcsecods.

Finally, with the results that could be calculated, one more comparison could be done by keeping the observation amount per second constant and changing the accuracy. These comparisons are shown in the Figures 4.20 and 4.21. It was evident in the figures that even though the improvement in the sensor accuracy effected the filter's estimations considerably, the effect of accuracy growth reduced after 0.01 *Arcsecond*, giving a sense that increasing accuracy further from this point would not help much.

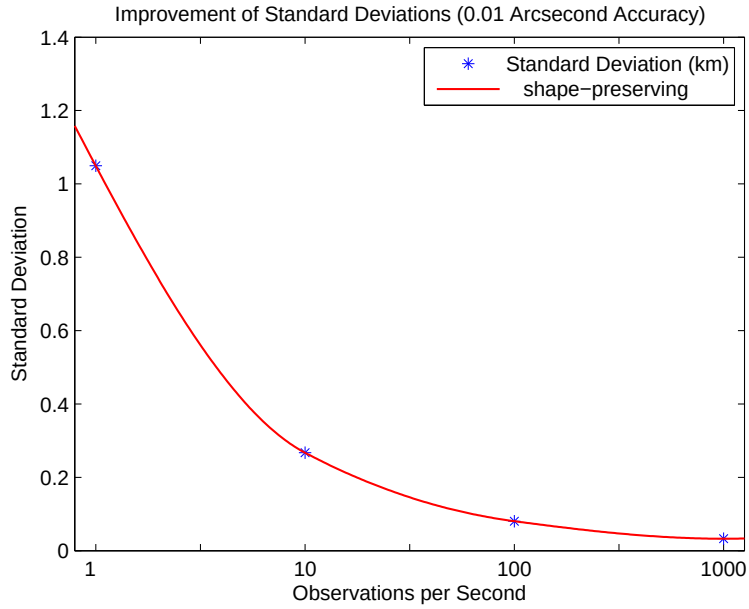

Figure 4.18: Improvement of Standard Deviation (0.01 Arcsecond Accuracy).

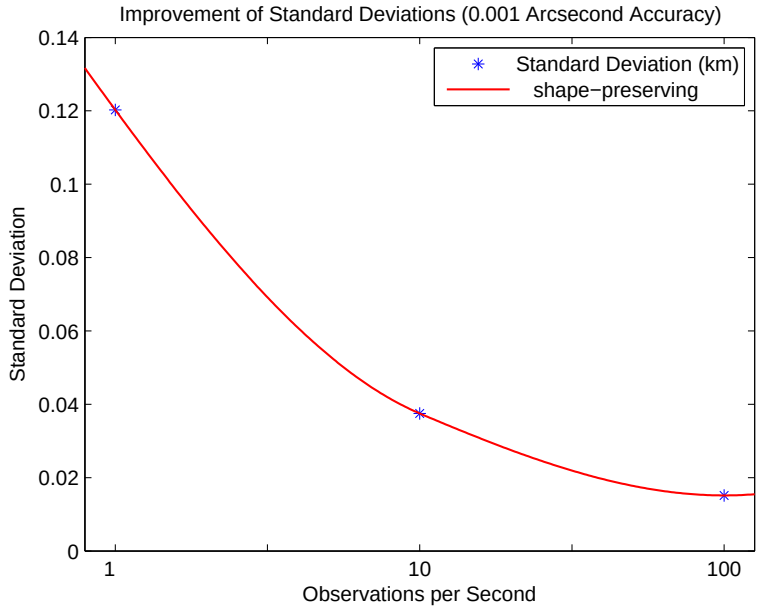

Figure 4.19: Improvement of Standard Deviation (0.001 Arcsecond Accuracy).

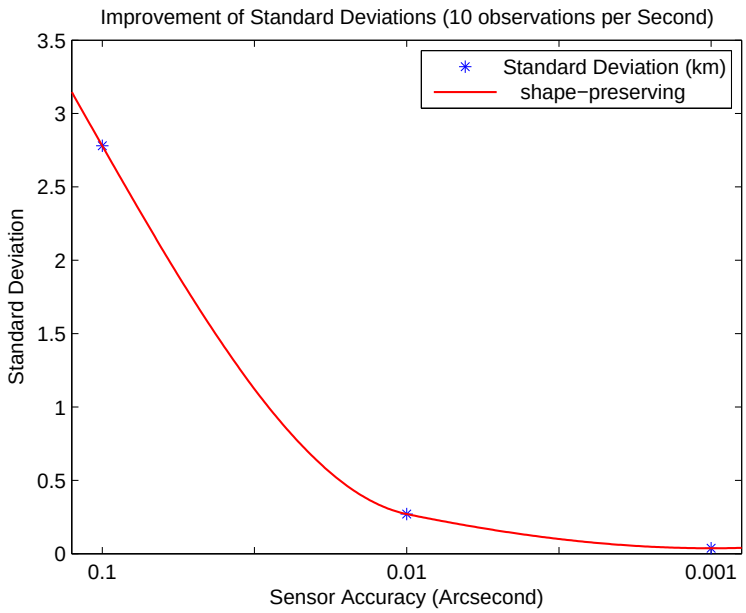

Figure 4.20: Improvement of Standard Deviation (10 Observations per Second).

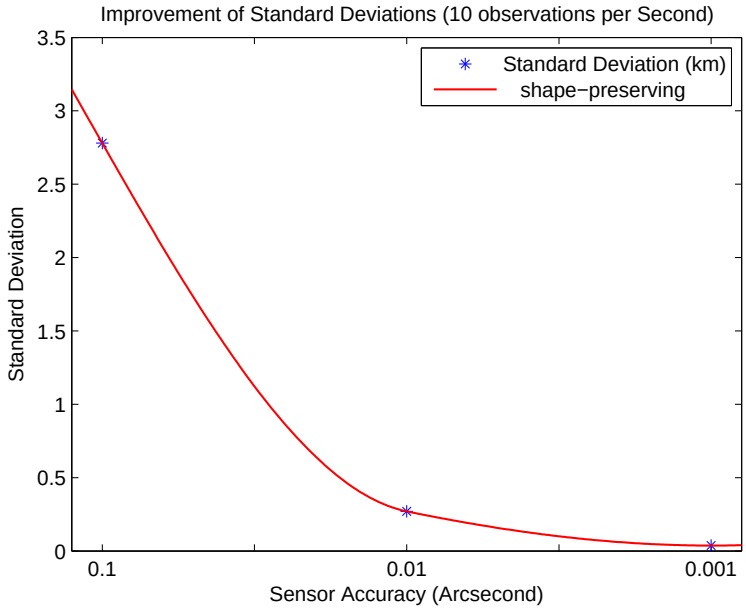

Figure 4.21: Improvement of Standard Deviation (100 Observations per Second).

V. Conclusions

5.1 Summary

This thesis demonstrates the ability to estimate the trajectory of a threat ASAT missile based on the angle-only observations conducted by a space-based onboard optical sensor. The importance of having a self defense capability for a satellite was emphasized with a brief description of the background of ASAT systems, space surveillance systems and the previous studies about this topic. This research aims to equip a space asset with an ability to first detect and track an ASAT missile and then estimate its future position with respect to its own position. Based on this capability the space asset would have a better situational awareness and probably have time for a last ditch maneuver to defeat the ASAT missile and survive. A least squares estimation filter was created and tested on a particular simulated scenario for different sensor specifications in order to determine the required sensor's capabilities.

5.2 Conclusions

The estimates of the filter were analyzed in the previous chapter. Since the observation inputs of the designed filter were provided by only one optical sensor and the sensor was assumed to perform angle-only measurements, it has been observed that the filter was highly limited due to the observability condition, as described in Chapter *III*. Simulation studies showed that the sensor accuracy should be at least 1 *Arcsecond* to be able to get an estimate from the filter which gets a maximum observation amount of 1000 observations per second. From another point of view the

sensor should perform at least one observations per second for the proper processing of this estimation filter using a sensor accuracy of maximum 1/1000 *Arcsecond*. These conclusions were for the case in which the sensor could perform observations from the very beginning until the impact point of the ASAT's trajectory.

To continue with the whole observation of the ASAT's trajectory case, the analysis of the simulations shows that if the sensor can perform 10 observations per second with an accuracy of 0.1 *Arcsecond* the standard deviations of the estimated miss distances in the radial axis (worst case) will be approximately 4.5 km. The satellite can maneuver out of this danger zone with an acceptable acceleration rate. Also it was observed that increasing the observation rate or the accuracy of the sensor beyond these values did not improve the results considerably. But with the consideration that the observations can be increased up to 100 hundred per second easily, this range can be reduced down to approximately 1.3km with using a sensor with the same accuracy of 0.1 *Arcsecond*.

Although the filter needs continuous observation of the ASAT in most cases, some more realistic cases could be generated to evaluate the capability of the filter and compare the possible sensor options. The main objective in these simulations was to leave the satellite some time before the impact to maneuver and also to consider the fact that the sensor can start the observations at some time after the launch. The simulations showed that the sensor accuracy should be at least 0.1 *Arcsecond* in order to be able to reduce observation data and have the filter generate an estimate within the observation amount and the sensor accuracy range that have been tested. Using

a 0.1 *Arcsecond* accurate sensor, the analysis showed that if it was assumed that the sensor could start performing observations 1 minute after the launch and stopped the observations 10 seconds before the impact time, with 100 observations per second the standard deviation of the estimated miss distances became $\approx 5\ km$. Assuming that the satellite could start the maneuver immediately, the defeat maneuver could be done with an acceleration rate of $\approx 10g's$. If the observation frequency was reduced to 10 observations per second and sensor accuracy was increased to be 0.01 *Arcsecond* then the required acceleration rate became $\approx 4g's$.

Finally, it was concluded that a space-based onboard sensor with an accuracy of 0.1 *Arcsecond* and the capability to perform 100 observations per second can establish the proposed operation for this specific scenario with reasonable results.

5.3 Future Work

During the simulations it has been discovered that the observability condition limits the filter estimates. If another observation can be added to the calculations the observability range can be enlarged. The research results can be improved by using the same filter and additional observation measurements. Additional observations can be performed by a sensor mounted on a geostationary satellite, mounted on a satellite in the same formation (if there is one) or another sensor on the same satellite with a lateral distance. Also, the effect of using an active optical sensor and a radar sensor on the estimations should be considered and calculated.

The perturbations on the two-body motion were not calculated in this research, so in a future work the effect of the perturbations and atmospheric effects should be included into the calculations. Also the observations obstructed by the curvature of the earth should be considered.

The simulations in this research were conducted using ordinary home-use computers. Based on this fact only a limited amount of simulations could be performed in a limited time. More sets of inputs can be generated, more simulations can be performed and the requirements of the optimum sensor can be determined in a narrower range if computers with faster processors and larger memories are used.

The non-linear least squares filter produced in this research is a batch filter and it has to wait until all of the data is available to make the estimate. In real life, the satellite would want to continuously update the estimate of the ASAT's trajectory. That would lead to a sequential type of filter like a Kalman Filter. As a start in this research topic, using a more stable filter like least squares to figure out the quality and the quantity requirements of the sensor was considered more appropriate. Given the recommendations for the quality and the quantity of the data, a possible future work will have a good starting point for working with the Kalman filter.

In real-time processing, it is important for the computer to "out run" real life. Also, in this scenario the faster the data comes in, the less time there is for the on-board computer to calculate the ASAT's trajectory. This is another reason to apply a sequential filter into these calculations. While working on the sequential

filtering, a future research should also examine whether a typical computer can "out run" realtime or not. [10]

This research examined only the case in which the ASAT was assumed to be an unguided ballistic missile. Precautions against other kind of ASAT systems like LASER ASATs or guided KE ASATs should be considered in the future studies.

Appendix A. MATLAB Code

A.1 Main Code

```
clc,clear,clf;

load data

du=6378.135;

tu=sqrt(6378.135^3/3.98601e5);

mu=1;

%%%%%%%%%%%%%%%%%%%%%%%%%%%%%%%%%%%%%%%%%%%%%%%%%%%%%%%%%%%%%%%%%%%%%%%

datapersec=100;    %enter observation amount per second

first=60           %enter fist second of data

last=10            %enter last data second (how many sec before impact)

accuracy=.001      %arcseconds

compute_z(datapersec);

%%%%%%%%%%%%%%%%%%%%%%%%%%%%%%%%%%%%%%%%%%%%%%%%%%%%%%%%%%%%%%%%%%%%%%%



firstdata=first*datapersec



if datapersec==1

load zQdata_1sec

z_i=z_i_1sec_p001(firstdata:length(z_1sec),:);

Q=Q_1sec_p001(firstdata:length(z_1sec),:);

lastdata=length(z_1sec)-firstdata-last*datapersec
```

```
end


if datapersec==10
load zQdata_1
z_i=z_i_1_p001(firstdata:length(asat1),:);
Q=Q_1_p001(firstdata:length(asat1),:);
lastdata=length(asat1)-firstdata-last*datapersec
end


if datapersec==25
load zQdata_p04sec
z_i=z_i_p04sec_p1(firstdata:length(z_p04sec),:);
Q=Q_p04sec_p1(firstdata:length(z_p04sec),:);
lastdata=length(z_p04sec)-firstdata-last*datapersec
end


if datapersec==100
load zQdata_01
z_i=z_i_01_p001(firstdata:length(asat02),:);
Q=Q_01_p001(firstdata:length(asat02),:);
lastdata=length(asat02)-firstdata-last*datapersec
end
```

```
for clmn=1:10

    [state_last,target]=statelast(firstdata,lastdata,z_i,Q,clmn,datapersec);

    clmn=clmn

    hold on

    [pos,pos_cross,pos_radial]=compute_r(state_last,clmn,target);

    hold on

    p_all(clmn)=pos;

    cross(clmn)=pos_cross;

    radial(clmn)=pos_radial;

end



[mean,stdev] = stat(p_all);

[mean_cross,stdev_cross] = stat(cross);

[mean_radial,stdev_radial] = stat(radial);


hold on
```

```
ellipsedraw(stdev_p1_p1_cross*du,stdev_p1_p1_radial*du,...
    mean_p1_p1_cross*du,mean_p1_p1_radial*du,0,'r');


hold on


xlabel('Cross Track Misdistance (Km.)    [b2------>(Earth)]')
ylabel('Radial Misdistance (Km.)    [b3------>(normal to orbital plane)]')
grid on
title('THE ASAT POSITION WITH RESPECT TO THE TARGET','FontSize',10)
str(1) = {['Data interval:',num2str(1/datapersec),'sec']};
str(2)={['SensorAccuracy:',num2str(accuracy),'Arcsec']};
str(3)={['FirstData:',num2str(first),'sec After Launch']};
str(4)={['LastData:',num2str(last),' sec to impact']};
str(5)={['Std.Dev.:',num2str(stdev*du),' Km']};
str(6)={['Std.Dev.CrossTrack:',num2str(stdev_cross*du),'Km']};
str(7)={['Std.Dev.Radial:',num2str(stdev_radial*du),'Km']};
str(8) = {'Ellipse : Std.Dev.-center at mean'};
h = axes('Position',[0 0 1 1],'Visible','off');
set(gcf,'CurrentAxes',h)
text(.65,.79,str,'FontSize',7)
```

A.2 MATLAB Functions Used in the Main Code

A.2.1 The Function to Create the Observations.

```
function [z_all]=compute_z(datapersec)


du=6378.135;

tu=sqrt(6378.135^3/3.98601e5);

mu=1;

load data


%%% 1/10 SECOND


if datapersec==10

asat=[asat1(:,4)/du asat1(:,5)/du asat1(:,6)/du];

t=[0:.1/tu:(((asat1(length(asat),1)-asat1(1,1))*24*3600)+.1)/tu];

target=[target1(:,4)/du target1(:,5)/du target1(:,6)/du ];

z_all=zeros(length(asat),100);

Q_all=zeros(length(asat),100);

for n=[1 .1 .01 .001];

    sigma_sens=n/3600*pi/180;

c=random('norm',0,sigma_sens,length(asat),100);

for k=1:length(asat)
```

```
    z(k,1)=abs((asat(k,1:3))*target(k,1:3)'/(norm(asat(k,1:3))*...
        norm(target(k,1:3))));



for m=1:100
    z_i(k,m)=z(k,1)+c(k,m)*sqrt(1-z(k,1)^2);
    if z_i(k,m)>1
       z_i(k,m)=z(k,1);
    end
    Q(k,m)=(sigma_sens^2)*(1-(z_i(k,m))^2);
end
end


z_all=[z_all z_i];
Q_all=[Q_all Q];
a=length(z_all(1,:))
end


z_1=z;
z_i_1_1=z_all(:,101:200);
z_i_1_p1=z_all(:,201:300);
z_i_1_p01=z_all(:,301:400);
```

```
z_i_1_p001=z_all(:,401:500);

Q_1_1=Q_all(:,101:200);

Q_1_p1=Q_all(:,201:300);

Q_1_p01=Q_all(:,301:400);

Q_1_p001=Q_all(:,401:500);

clear z_all Q_all a target t asat asat1 asat02...

    asat002 target1 target02 target002 c k mu du tu sigma_sens m n z

save zQdata_1

end


%%% 1/100 SECOND


if datapersec==100

k=1;

asat=[asat02(:,4)/du asat02(:,5)/du asat02(:,6)/du];

target=[target02(:,4)/du target02(:,5)/du target02(:,6)/du];

z_all=zeros(length(asat),10);

Q_all=zeros(length(asat),10);

for n=[1 10 100 .1 .01 .001];

    sigma_sens=n/3600*pi/180;

    c=random('norm',0,sigma_sens,length(asat),10);

    for k=1:length(asat)
```

```
z(k,1)=(asat(k,1:3))*target(k,1:3)'/(norm(asat(k,1:3))*...
    norm(target(k,1:3)));



        for m=1:10


            z_i(k,m)=z(k,1)+c(k,m)*sqrt(1-z(k,1)^2);
            if z_i(k,m)>1
               z_i(k,m)=z(k,1);
            end
            Q(k,m)=(sigma_sens^2)*(1-(z_i(k,m))^2);
        end
    end
    z_all=[z_all z_i];
    Q_all=[Q_all Q];
    a=length(z_all(1,:))
end
z_01=z;
z_i_01_1=z_all(:,11:20);
z_i_01_10=z_all(:,21:30);
z_i_01_100=z_all(:,31:40);
z_i_01_p1=z_all(:,41:50);
```

```
z_i_01_p01=z_all(:,51:60);

z_i_01_p001=z_all(:,61:70);

Q_01_1=Q_all(:,11:20);

Q_01_10=Q_all(:,21:30);

Q_01_100=Q_all(:,31:40);

Q_01_p1=Q_all(:,41:50);

Q_01_p01=Q_all(:,51:60);

Q_01_p001=Q_all(:,61:70);


clear z_all Q_all a target t asat asat1 asat02 asat002...

    target1 target02 target002 c k mu du tu sigma_sens m n z

save zQdata_01


end




du=6378.135;

tu=sqrt(6378.135^3/3.98601e5);

mu=1;

load data
```

```
%%%%%%%%%%%%%%%%%%%%%%%%%%%%%%%%%%%%%%%%%%

%%%  1SECOND
if datapersec==1
for j=0:524;
  asat(j+1,1:6)=[asat1(10*j+1,4)/du asat1(10*j+1,5)/du...
       asat1(10*j+1,6)/du asat1(10*j+1,7)*tu/du asat1(10*j+1,8)*tu/du...
       asat1(10*j+1,9)*tu/du];
  target(j+1,1:6)=[target1(10*j+1,4)/du target1(10*j+1,5)/du...
        target1(10*j+1,6)/du target1(10*j+1,7)*tu/du...
        target1(10*j+1,8)*tu/du target1(10*j+1,9)*tu/du];
end
t=[0:1/tu:j/tu];
z_all=zeros(length(asat),100);
Q_all=zeros(length(asat),100);
for n=[1 .1 .01 .001];
    sigma_sens=n/3600*pi/180;
    c=random('norm',0,sigma_sens,length(asat),100);
    for k=1:length(asat)
    z(k,1)=abs((asat(k,1:3))*target(k,1:3)'/(norm(asat(k,1:3))*...
        norm(target(k,1:3))));
```

```
    for m=1:100


        z_i(k,m)=z(k,1)+c(k,m)*sqrt(1-z(k,1)^2);
        if z_i(k,m)>1
           z_i(k,m)=z(k,1);
        end
        Q(k,m)=(sigma_sens^2)*(1-(z_i(k,m))^2);
    end


end


z_all=[z_all z_i];
Q_all=[Q_all Q];
a=length(z_all(1,:))
end


z_1sec=z;
z_i_1sec_1=z_all(:,101:200);
z_i_1sec_p1=z_all(:,201:300);
z_i_1sec_p01=z_all(:,301:400);
z_i_1sec_p001=z_all(:,401:500);
clear z_all
```

```
Q_1sec_1=Q_all(:,101:200);

Q_1sec_p1=Q_all(:,201:300);

Q_1sec_p01=Q_all(:,301:400);

Q_1sec_p001=Q_all(:,401:500);


clear z_all Q_all a target t asat asat1 asat02 asat002...

    target1 target02 target002 c k mu du tu sigma_sens m n z

save zQdata_1sec

end
```

A.2.2 The Function to Compute the Estimated State at the Impact Time.

```
function [state_last,target]=statelast(firstdata,lastdata,z_i,...

Q,clmn,datapersec)


delta_x=1e20*[1;1;1;1;1;1];

P=eye(6);


%using canonical units

du=6378.135;

tu=sqrt(6378.135^3/3.98601e5);

mu=1;
```

```
load data


%%% 1 SECOND

if datapersec==1

for j=0:524;

asat(j+1,1:6)=[asat1(10*j+1,4)/du asat1(10*j+1,5)/du...

asat1(10*j+1,6)/du ...

asat1(10*j+1,7)*tu/du asat1(10*j+1,8)*tu/du...

asat1(10*j+1,9)*tu/du];

target(j+1,1:6)=[target1(10*j+1,4)/du target1(10*j+1,5)/du...

target1(10*j+1,6)/du target1(10*j+1,7)*tu/du...

target1(10*j+1,8)*tu/du target1(10*j+1,9)*tu/du];

end

target=[target(firstdata:length(asat),1)...

target(firstdata:length(asat),2)...

target(firstdata:length(asat),3) ...

target(firstdata:length(asat),4)...

target(firstdata:length(asat),5)...

target(firstdata:length(asat),6)];

asat=[asat(firstdata:length(asat),1)...

asat(firstdata:length(asat),2)...
```

```
asat(firstdata:length(asat),3) ...

asat(firstdata:length(asat),4)...

asat(firstdata:length(asat),5)...

 asat(firstdata:length(asat),6)];

t=[0:1/tu:(length(asat)-1)/tu];

state_zero=[asat(1,1) asat(1,2) asat(1,3) asat(1,4) asat(1,5) asat(1,6)]';


end



%%% 1/10 SECOND

if datapersec==10

asat=[asat1(firstdata:length(asat1),4)/du ...

asat1(firstdata:length(asat1),5)/du ...

asat1(firstdata:length(asat1),6)/du ...

asat1(firstdata:length(asat1),7)*tu/du...

asat1(firstdata:length(asat1),8)*tu/du...

asat1(firstdata:length(asat1),9)*tu/du];

t=[0:.1/tu:(((asat1(length(asat1),1)-...

asat1(firstdata,1))*24*3600)+.1)/tu];

target=[target1(firstdata:length(asat1),4)/du...

target1(firstdata:length(asat1),5)/du...
```

```
target1(firstdata:length(asat1),6)/du ...

target1(firstdata:length(asat1),7)*tu/du...

target1(firstdata:length(asat1),8)*tu/du...

 target1(firstdata:length(asat1),9)*tu/du];

state_zero=[asat(1,1) asat(1,2) asat(1,3) asat(1,4) asat(1,5) asat(1,6)]';


end



%%% 1/100 SECOND

if datapersec==100


asat=[asat02(firstdata:length(asat02),4)/du...

asat02(firstdata:length(asat02),5)/du...

asat02(firstdata:length(asat02),6)/du ...

asat02(firstdata:length(asat02),7)*tu/du...

asat02(firstdata:length(asat02),8)*tu/du...

asat02(firstdata:length(asat02),9)*tu/du];

t=[0:.01/tu:(((asat02(length(asat02),1)-...

asat02(firstdata,1))*24*3600)+.01)/tu];

target=[target02(firstdata:length(asat02),4)/du...

target02(firstdata:length(asat02),5)/du...
```

```
target02(firstdata:length(asat02),6)/du ...

target02(firstdata:length(asat02),7)*tu/du...

target02(firstdata:length(asat02),8)*tu/du...

target02(firstdata:length(asat02),9)*tu/du];

state_zero=[asat(1,1) asat(1,2) asat(1,3) asat(1,4) asat(1,5) asat(1,6)]';

end









%%%%%%%%%%%%%%%%%%%%%%%%%%%%%%%%%%%%%%%%%%%%%%%%%%%%%%%%%%%%%%%%%%%%%%%%%%%%

state_new=state_zero;


while length(nonzeros(delta_x<.1*sqrt(diag(P))))<6


state_zero=state_new

phi_zero=[1 zeros(1,6) 1 zeros(1,6) 1 zeros(1,6) 1 zeros(1,6) 1...

 zeros(1,6) 1]';

y_zero=[phi_zero;state_zero]';


[t,y]=ode45(@y_eom_1,t,y_zero);
```

```
P_inv=0;

residual=0;

rsdl_sum=0;

delta_x=0;


 for i=(1:length(t))

        state(i,1:6)=y(i,37:42);


        phi=[y(i,1) y(i,2) y(i,3) y(i,4) y(i,5) y(i,6);...

        y(i,7) y(i,8) y(i,9) y(i,10) y(i,11) y(i,12);...

        y(i,13) y(i,14) y(i,15) y(i,16) y(i,17) y(i,18);...

        y(i,19) y(i,20) y(i,21) y(i,22) y(i,23) y(i,24);...

        y(i,25) y(i,26) y(i,27) y(i,28) y(i,29) y(i,30);...

        y(i,31) y(i,32) y(i,33) y(i,34) y(i,35) y(i,36);];



        denum=sqrt((state(i,1)^2+state(i,2)^2+state(i,3)^2)*...

        (target(i,1)^2+target(i,2)^2+target(i,3)^2));

        num=state(i,1)*target(i,1)+state(i,2)*target(i,2)+...

        state(i,3)*target(i,3);

        r_target_2=(target(i,1)^2+target(i,2)^2+target(i,3)^2);
```

```
        H=[-state(i,1)*num*r_target_2/denum^3+target(i,1)/denum ...
           -state(i,2)*num*r_target_2/denum^3+target(i,2)/denum ...
           -state(i,3)*num*r_target_2/denum^3+target(i,3)/denum ...
                                          0 ...
                                          0 ...
                                          0];



% computing residuals
  G(i,1:1)=state(i,1:3)*target(i,1:3)'/(norm(state(i,1:3))*...
  norm(target(i,1:3)));
  rsdl(i,1:1)=z_i(i,clmn)-G(i,1:1);


  T=H*phi;


  P_inv_1=T'*inv(Q(i,clmn))*T;
  rsdl_sum_1=T'*inv(Q(i,clmn))*rsdl(i,1:1);



    if i>lastdata
        P_inv_1=0;
```

```
        rsdl_sum_1=0;

    end


  P_inv=P_inv+P_inv_1;

  rsdl_sum= rsdl_sum+rsdl_sum_1;


   end


P=inv(P_inv);

delta_x=P*rsdl_sum;

dbstop if warning

state_new=state(1,1:6)'+delta_x;

clear  y rsdl  state


end


[t,x]=ode45(@state_eom,t,state_new);


state_last(:,1:6)=x(:,1:6);

clear x
```

A.2.3 The Function to Compute the Estimated State at the Impact Time with Respect to the Body Frame.

```
function [pos,pos_cross,pos_radial]=compute_r(state_last,clmn,target)


du=6378.135;

tu=sqrt(6378.135^3/3.98601e5);

mu=1;


b1=target(length(state_last),4:6)/norm(target(length(state_last),4:6));

b3=cross(b1,target(length(state_last),1:3)...

    /norm(target(length(state_last),1:3)));

b3=b3/norm(b3);

b2=cross(b1,b3);

R_ib=[b1' b2' b3'];

R_bi=R_ib';


state_body=R_bi*(state_last(length(state_last),1:3)-...

    target(length(state_last),1:3))';


pos=norm(state_body(2),state_body(3));

pos_cross=state_body(2);

pos_radial=state_body(3);
```

```
figure(1)
line([0 0],[0 0],'Marker','d','Markerfacecolor','r','LineStyle'...
    ,'none','color','r')
line([state_body(2)*du 0],[state_body(3)*du 0],'Marker','*',...
    'LineStyle','none','color','b')

clear state_last
```

A.2.4 The Function to Iterate the State and the Φ Matrix in Time.

```
function y_dot=y_eom_1(t,y)
mu=1;

X=y(37);
Y=y(38);
Z=y(39);
r=sqrt(X^2+Y^2+Z^2);

B=[zeros(3) eye(3);(-mu/r^3)*eye(3) zeros(3)];

A_rr=[(-mu/(r^3))+((3*mu*X^2)/(r^5)) (3*mu*X*Y)/(r^5) (3*mu*X*Z)/(r^5);...
```

```
      (3*mu*X*Y)/(r^5) (-mu/(r^3))+((3*mu*Y^2)/(r^5)) (3*mu*Y*Z)/(r^5);...
      (3*mu*X*Z)/(r^5) (3*mu*Y*Z)/(r^5) (-mu/(r^3))+((3*mu*Z^2)/(r^5))];
A=[zeros(3) eye(3);A_rr zeros(3)];

AA=[A(1,1)*eye(6) A(1,2)*eye(6) A(1,3)*eye(6) A(1,4)*eye(6)...
    A(1,5)*eye(6) A(1,6)*eye(6);...
A(2,1)*eye(6) A(2,2)*eye(6) A(2,3)*eye(6) A(2,4)*eye(6)...
A(2,5)*eye(6) A(2,6)*eye(6);...
A(3,1)*eye(6) A(3,2)*eye(6) A(3,3)*eye(6) A(3,4)*eye(6)...
A(3,5)*eye(6) A(3,6)*eye(6);...
A(4,1)*eye(6) A(4,2)*eye(6) A(4,3)*eye(6) A(4,4)*eye(6)...
A(4,5)*eye(6) A(4,6)*eye(6);...
A(5,1)*eye(6) A(5,2)*eye(6) A(5,3)*eye(6) A(5,4)*eye(6)...
A(5,5)*eye(6) A(5,6)*eye(6);...
A(6,1)*eye(6) A(6,2)*eye(6) A(6,3)*eye(6) A(6,4)*eye(6)...
A(6,5)*eye(6) A(6,6)*eye(6);];

AAA=[AA zeros(36,6);zeros(6,36) B];
y_dot=AAA*y;
end
```

A.2.5 The Function to Compute the Mean and the Standard Deviation Values.

```
function [mean,stdev] = stat(x)

n = length(x);

mean = sum(x)/n;

stdev = sqrt(sum((x-mean).^2/n));
```

Bibliography

1. "Ballistic Missile Defense Organisation". Excerpt from unpublished article. n. pag., january 2008. URL `http://www.mda.mil`. Fact Sheets.

2. "Gaussian Distribution Function". Excerpt from unpublished article. n. pag., january 2008. URL `http://www.to.infn.it/ zaninett/javascript/distributions/`$gaussiana_b.html$. Picture was taken from the site and modified.

3. "Johnson Island". Excerpt from unpublished article. n. pag., January 2008. URL $http : //community - 2.webtv.net/@HH!B1!D5!52C2BB1B304E/CobraBall/JohnstonIsland/$.

4. Annie B. Mclaughlin, Jason S. Prichett John H. Stone Gregory K. VanDyk, Jesse T. Mclaughlin. *Protection Of A High Valued Space Asset*. Master's thesis, Graduate School of Engineering, Air Force Institute of Technology (AETC), Wright-Patterson AFB OH, March 2007. AFIT/GSE/ENV/07-M04.

5. C.B.Chang. "Ballistic Trajectory Estimation with Angle-only Measurements". *Transactions on Automatic Control*, 474–480. June 1980.

6. Dr.T.S.Kelso. "Space Debris Chinese ASAT Test Adds More to the Clutter". Excerpt from unpublished article. n. pag., April 2007. URL `http://www.agi.com`. AGI online Web seminar.

7. Grant H. Stokes, Ramaswamy Sridharan David Harrison, Curt von Braun and Jayant Sharma. "Space-based Visual Program". *Lincoln Laboratuary Journal*, 11(2), 1998.

8. Grego, Laura. "A History of Anti-Satellite Weapons Programs". Excerpt from unpublished article. n. pag., May 2006. URL `http://www.ucsusa.org/global-security/space-weapons.html`. Union of Concerned Scientists.

9. Hicks, Kerry D. *An Autonomous Orbit Determination System for Earth Satellites*. Ph.D. dissertation, Graduate School of Engineering, Air Force Institute of Technology (AETC), Wright-Patterson AFB OH, November 1989. AFIT/DS/AA/89-01.

10. Hicks, Kerry D. Excerpt from discussions about the possible future works for the resarch., Feb 2008.

11. John Pike, Robert Sherman. "Space Surveillance". Excerpt from unpublished article. n. pag., 20 April 1997. URL `http://www.fas.org/spp/military/program/track/overview.htm`. Federation of American Scientists.

12. John Pike, Steven Aftergood. "Anti-Satellite Weapons". Excerpt from unpublished article. n. pag., 23 May 2007. URL `http://www.fas.org/spp/military/program/asat/index.html`. Federation of American Scientists.

13. Kelso, Dr.T.S. *Satellite Times*, (1), September/October.

14. Klinkrad, H. "Monitoring Space,Efforts Made By Europian Countries". Excerpt from unpublished article. n. pag., January 2008. URL `http://www.fas.org/spp/military/program/track/klinkrad.pdf`. Federation of American Scientists.

15. Murali Yeddanapudi, Khishna R. Pattipati Somnath Deb, Yaakov Bar-shalom. "Ballistic Missile Track Initiation From Satellite Observations". *Transactions on Aerospace and Electronic Systems*, 1054–1071. July 1995.

16. Nordlie, John. *The Rise, Fall, and Rebirth of Anti-satellite Weapons*. Technical report, University of North Dakota, 1992. URL *http : //blizzard.rwic.und.edu/ nordlie/papers/asat.html*. For Military Applications of Space course.

17. O'Brien, Daniel L. *Preliminary Design Of A Model To Assess The Effect Of SSN Sensor Upgrades On Orbit Prediction Accuracies Relative To The U.S. ASAT Mission*. Master's thesis, Graduate School of Engineering, Air Force Institute of Technology (AETC), Wright-Patterson AFB OH, December 1991. AFIT/GSO/ENS/ENY/91D-14.

18. Roger R. Bate, Jerry E. White, Donald D. Mueller. *Fundamentals of Astrodynamics*. Dover Publications, Inc., 180 Varick Street, New York, NY, 1971.

19. Watkins, Sharon. "What was NIKE-ZEUS". *The Eagle*, 14(2), 2007.

20. Wiesel, William E. *Modern Orbit Determination*. Aphelion Press, 2652 Yalonda Ct., Beavercreek, OH, 2003.

21. Wiley J. Larson, James R. Wertz. *Space Mission Analysis and Design*. Microcrosm Press, Kluwer Academic Publishers, 401 Coral Circle, El Segundo,CA, 2005.

Vita

Mesut Gülmüş was born in 1978 in Bursa, Türkiye. Upon graduating from Bursa Anatolian High School in 1996, he attended to the Turkish Air Force Academy in 1996. He graduated from the TUAF with Aeronautical Engineering degree in 2000. His first assignment was at Çiğli/İzmir 2nd Air Training Base as a pilot trainee. He completed his pilot training as an F-16 pilot. In 2003 he was assigned to the 162^{th} Flight Squadron in Bandırma . In September 2006, he entered the Graduate School of Engineering and Management, Air Force Institute of Technology. Upon graduation, he will be assigned to the 162^{th} Flight Squadron back.

REPORT DOCUMENTATION PAGE

Form Approved
OMB No. 0704–0188

1. REPORT DATE *(DD–MM–YYYY)*	2. REPORT TYPE	3. DATES COVERED *(From — To)*
06–03–2008	Master's Thesis	Sept 2006 — Mar 2008

4. TITLE AND SUBTITLE

Determining the capability requirements for a space based optical sensor to determine the trajectory of an incoming antisatellite weapon

5a. CONTRACT NUMBER

DACA99–99–C–9999

5b. GRANT NUMBER

5c. PROGRAM ELEMENT NUMBER

6. AUTHOR(S)

Mesut GÜLMÜŞ

5d. PROJECT NUMBER

5e. TASK NUMBER

5f. WORK UNIT NUMBER

7. PERFORMING ORGANIZATION NAME(S) AND ADDRESS(ES)

Air Force Institute of Technology
Graduate School of Engineering and Management (AFIT/EN)
2950 Hobson Way
WPAFB OH 45433-7765

8. PERFORMING ORGANIZATION REPORT NUMBER

AFIT/GE/ENY/08M-03

9. SPONSORING / MONITORING AGENCY NAME(S) AND ADDRESS(ES)

10. SPONSOR/MONITOR'S ACRONYM(S)

11. SPONSOR/MONITOR'S REPORT NUMBER(S)

12. DISTRIBUTION / AVAILABILITY STATEMENT

Approval for public release; distribution is unlimited.

13. SUPPLEMENTARY NOTES

14. ABSTRACT

The goal of this research is to build up a logic to catch and track the incoming ASAT weapons by using space-based onboard optical sensors. The satellite orbit and ASAT trajectory of the Chinese test were generated to relate the research to the real world application. These position and velocity values are used to generate simulated observation data for the imaginary sensor on the targeted satellite. These observation values are assumed to be true, and some representative amounts of error is added to these data. Only two body dynamics are considered, drag effect and other perturbations are neglected. The modern orbit determination process, least squares method, and Monte Carlo techniques are used to calculate the estimated orbit of the ASAT. Standard deviations of the relative position of the ASAT with respect to the targeted satellite at the time of impact are calculated for different sensors with different accuracy and data collection intervals.

15. SUBJECT TERMS

ASAT, anti-satellite, orbit determination, least squares

16. SECURITY CLASSIFICATION OF:			17. LIMITATION OF ABSTRACT	18. NUMBER OF PAGES	19a. NAME OF RESPONSIBLE PERSON
a. REPORT	b. ABSTRACT	c. THIS PAGE			Lt Col Kerry D Hicks
U	U	U	UU	115	19b. TELEPHONE NUMBER *(include area code)* (937) 255–3636, ext 4644